Geosci. Model Dev. Discuss., https://doi.org/10.5194/gmd-2017-191
Manuscript under review for journal Geosci. Model Dev.
Discussion started: 3 November 2017

Geoscientific Model Development Discussions

The Chemistry Climate Model ECHAM6.3-HAM2.3-MOZ1.0

Martin G. Schultz[1,a], Scarlet Stadtler[1], Sabine Schröder[1], Domenico Taraborrelli[1], Bruno Franco[1,b], Jonathan Krefting[2], Alexandra Henrot[3], Sylvaine Ferrachat[4], Ulrike Lohmann[4], David Neubauer[4], Colombe Siegenthaler-Le Drian[5], Sebastian Wahl[6], Harri Kokkola[7], Thomas Kühn[7], Sebastian Rast[8], Hauke Schmidt[8], Philip Stier[9], Doug Kinnison[10], Geoffrey S. Tyndall[10], John J. Orlando[10], and Catherine Wespes[11]

[1]Institut für Energie- und Klimaforschung, IEK-8, Forschungszentrum Jülich, Germany
[2]Meteorologisches Institut, Universität Bonn, Bonn, Germany
[3]Unité de Modélisation du Climat et des Cycles Biogéochimiques, University of Liège, Liège, Belgium
[4]Institute for Atmospheric and Climate Science, ETH Zurich, Zurich, Switzerland
[5]Centre for Climate Systems Modeling (C2SM), ETH Zurich, Switzerland
[6]GEOMAR Helmholtz Centre for Ocean Research Kiel, Kiel, Germany
[7]Finnish Meteorological Institute, Atmospheric Research Centre of Eastern Finland, Kuopio, Finland
[8]Max Planck Institute for Meteorology, Hamburg, Germany
[9]Atmospheric, Oceanic and Planetary Physics, Department of Physics, University of Oxford, Oxford, United Kingdom
[10]NCAR, Atmospheric Chemistry Observations & Modeling, Boulder, CO, USA
[11]Universite Libre de Bruxelles, Brussels, Belgium
[a]now at Jülich Supercomputing Centre, Forschungszentrum Jülich, Germany
[b]now at Universite Libre de Bruxelles, Brussels, Belgium

Correspondence to: Martin G. Schultz (m.schultz@fz-juelich.de)

Abstract. The chemistry climate model ECHAM-HAMMOZ contains a detailed representation of tropospheric and stratospheric reactive chemistry and state-of-the-art parametrisations of aerorols using either a modal scheme (M7) or a bin scheme (SALSA). This article describes and evaluates the model version ECHAM6.3-HAM2.3-MOZ1.0 with a focus on the tropospheric gas-phase chemistry. A ten-year model simulation was performed to test the stability of the model and provide data for its evaluation. The comparison to observations concentrates on the year 2008 and includes total column observations of ozone (O_3) and carbon monoxide (CO) from Infrared Atmospheric Sounding Interferometer (IASI) and Ozone Monitoring Instrument (OMI), Microwave Limb Sounder (MLS) observations of temperature, nitric acid (HNO_3), chlorine monoxide (ClO), and O_3 for the evaluation of polar stratospheric processes, an ozone sonde climatology, surface ozone observations from the Tropospheric Ozone Assessment Report (TOAR) database, and surface CO data from the Global Atmosphere Watch network. Global budgets of ozone, hydroxide (OH), nitrogen oxides (NO_x), aerosols, clouds, and radiation are analyzed and compared to the literature. ECHAM-HAMMOZ performs well in many aspects. However, in the base simulation, lightning NO_x emissions are very low, and the impact of the heterogeneous reaction of HNO_3 on dust and seasalt aerosol is too strong. Sensitivity simulations with increased lightning NO_x or modified heterogeneous chemistry deteriorate the comparison with observations and yield excessively large ozone budget terms and too much OH. We hypothesize that this is an impact of potential issues with tropical convection in the ECHAM model.

Geosci. Model Dev. Discuss., https://doi.org/10.5194/gmd-2017-191
Manuscript under review for journal Geosci. Model Dev.
Discussion started: 3 November 2017

Geoscientific Model Development Discussions
Open Access
EGU

Geosci. Model Dev. Discuss., https://doi.org/10.5194/gmd-2017-191
Manuscript under review for journal Geosci. Model Dev.
Discussion started: 3 November 2017

Geoscientific Model Development Discussions

1 Introduction

Global chemistry climate models have become indispensible tools for the investigation of interactions between atmospheric chemistry and various aspects of the physical and biogeochemical climate system. In recent years, several coupled models have been developed with varying levels of interaction between Earth System components and varying details in their representation of chemical and physical processes (cf. Eyring et al., 2013; Young et al., 2013).

Here, we describe and evaluate a new chemistry climate model based on the general circulation model ECHAM6.3 (Stevens et al., 2013), the Hamburg Aerosol Model (HAM) version 2.3 (Stier et al., 2005; Zhang et al., 2012, Neubauer et al., in preparation), and the gas-phase tropospheric and stratospheric module MOZ1.0.

ECHAM6.3-HAM2.3-MOZ1.0 (henceforth ECHAM-HAMMOZ) can be run in different configurations: (1) using prescribed fields of surface pressure, divergence, vorticity, and temperature, and applying a relaxation technique with time-varying weights ("nudging"); (2) constraining only sea-surface temperatures and sea-ice concentrations ("AMIP mode"); or (3) fully-coupled with ocean and sea-ice models. In this study we concentrate on simulations of type 1 as these allow for a more detailed evaluation of the model with observational data and because most current applications of ECHAM-HAMMOZ use this mode. Possible differences between the different configurations are discussed elsewhere (for example Lamarque et al., 2012).

Earlier versions of ECHAM-HAMMOZ have been used successfully to analyze the impact of heterogeneous reactions on tropospheric ozone chemistry (Pozzoli et al., 2008a) and on aerosol composition (Pozzoli et al., 2008b) over the North Pacific, the influence of African emissions on regional and global tropospheric ozone (Aghedo et al., 2007), the impact of continental pollution outflow on the chemical tendencies of ozone (Auvray et al., 2007), and the impact of Asian aerosol and trace gas emissions on the Asian monsoon (Fadnavis et al., 2013, 2014, 2015). A 25-year reanalysis with ECHAM-HAMMOZ was performed by Pozzoli et al. (2011). In addition, several studies were performed with the aerosol climate model ECHAM-HAM-M7, which uses trace gas climatologies from ECHAM-HAMMOZ to constrain aerosol nucleation (e.g., Jiao et al., 2014; Neubauer et al., 2014; Stanelle et al., 2014; Ghan et al., 2016; Zhang et al., 2016). The tropospheric chemistry climate model ECHAM5-MOZ also participated in the first multi-model intercomparison study of the Task Force Hemispheric Transport of Air Pollutants (TFHTAP; Dentener et al., 2006a; Stevenson et al., 2006).

This article intends to provide a thorough description of the chemistry component of the ECHAM-HAMMOZ model with special focus on tropospheric reactive gases. Stratospheric chemistry is briefly discussed as well, while for more detailed discussions of the performance of the physical climate model ECHAM6.3 the reader is referred to Stevens et al. (2013). More information on the aerosol schemes HAM-M7 and HAM-SALSA and their evaluation can be found in Stier et al. (2005), Zhang et al. (2012), Neubauer et al. (2014), Neubauer et al. (in preparation), Kokkola et al. (in preparation), and Tgeen et al., in preparation, respectively.

This article first provides general descriptions of the ECHAM6.3, HAM2.3, and MOZ1.0 components (section 2) before the gas-phase chemistry parameterisations are discussed in more detail (section 3). Section 4 provides an overview of the simulations performed for this paper. Section 5 presents simulation results and comparisons with observations and other,

Geosci. Model Dev. Discuss., https://doi.org/10.5194/gmd-2017-191
Manuscript under review for journal Geosci. Model Dev.
Discussion started: 3 November 2017

independent model simulations. In section 6 we analyze the global budgets of ozone, OH, NO_x, aerosols, clouds, and radiation. Section 7 contains conclusions.

2 Model description

2.1 ECHAM6.3

ECHAM6, subversion 3, is the sixth generation general circulation model from the Max Planck Institute for Meteorology in Hamburg, Germany (Stevens et al., 2013). The model uses a spectral dynamical core to calculate temperature, surface pressure, vorticity, and divergence. Diabatic processes such as convection, diffusion, turbulence, gravity waves, etc. are calculated on an associated Gaussian grid. The vertical discretization is a hybrid sigma-pressure coordinate system. Typical model resolutions of ECHAM6.3 are T63L47, T63L95, and T106L95, where T_N denotes the triangular truncation, and L_M specifies the number of vertical levels. Simulations in T255L95 and T31L47 are also possible.

Transport of scalar quantities is performed with the flux-form semi-Lagrangian scheme of Lin and Rood (1996). Turbulent mixing adopts an eddy diffusivity/viscosity approach following Brinkop and Roeckner (1995), moist convection is parameterized according to Tiedtke (1989) with extensions by Nordeng (1994) and Möbis and Stevens (2012). Stratiform clouds are computed diagnostically based on a relative humidity threshold (Sundqvist et al., 1989). Cloud water and cloud ice are treated prognostically according to Lohmann and Roeckner (1996). In the base model version, the cloud droplet number concentration is parameterized as a function of altitude with higher values over land than over the ocean.In contrast, ECHAM-HAMMOZ explicitly calculates cloud droplet number concentration as a function of aerosol activation (see below). Gravity waves are generated from a subgrid orography scheme (Lott, 1999), and as Doppler waves following Hines (1997a, b), and they are treated according to the formulation of Palmer et al. (1986) and Miller et al. (1989). Radiative transfer calculations are done with the two-stream method of RRTM-G (Iacono et al., 2008). The optical properties for radiation are updated every 2 hours. In contrast to the base model version, which applies climatological fields for this purpose, the radiation calculation of ECHAM-HAMMOZ uses the prognostic tracer concentrations of aerosol and the following gases to specify absorption and scattering: CO_2, CH_4, N_2O, CFC11, CFC12, O_2, O_3. Cloud scattering is parameterized according to Mie theory using maximum-random cloud overlap and an inhomogeneity parameter to account for three-dimensional effects. Surface albedo is parameterized according to Brovkin et al. (2013).

Land surface processes are modeled with JSBACH (Reick et al., 2013), which uses a tiling approach with 12 plant functional types and two types of bare surface. The soil hydrology and temperatures are modeled by a five-layer scheme (Hagemann and Stacke, 2015), which constitutes an update from the description provided by Stevens et al. (2013).

2.2 HAM2.3

The Hamburg Aerosol Model HAM consists of parametrizations of all relevant aerosol processes including emissions, nucleation, condensation, coagulation, cloud activation, dry deposition, wet deposition and sedimentation. HAM solves prognostic

Geosci. Model Dev. Discuss., https://doi.org/10.5194/gmd-2017-191
Manuscript under review for journal Geosci. Model Dev.
Discussion started: 3 November 2017

equations for sulfate, black carbon, particulate organic matter, sea salt and mineral dust aerosol. Two different representations of aerosol microphysics are available based on the modal scheme M7 (Vignati et al., 2004; Stier et al., 2005), or on the Sectional Aerosol module for Large Scale Applications ("SALSA": Kokkola et al., 2008; Bergman et al., 2012). The simulations described in this paper were performed with the SALSA scheme. Interactions with clouds are implemented through a two-moment cloud microphysics scheme (Lohmann et al., 2007; Lohmann and Hoose, 2009) with prognostic variables for cloud droplet number concentration (CDNC) and ice crystal number concentration (ICNC). Emissions, dry and wet deposition are handled consistently between the aerosol scheme and the gas-phase chemistry scheme MOZ (see section 2.3).

SALSA represents aerosol sizes as 10 size bins, which are grouped into three ranges with 3 bins from 3 nm to 50 nm, 4 bins from 50 nm to 700 nm, and 3 bins from 700 nm to 10 $\mu\mathrm{m}$. Within each group, the size bins are logarithmically equally spaced. The aerosol size distribution is further divided into a soluble and an insoluble aerosol population. Insoluble particles only occur in the largest seven bins. SALSA solves the microphysical processes of nucleation, condensation, coagulation, and hydration. To accommodate SALSA, aerosol processes, which are handled by HAMMOZ, i.e. emissions, wet and dry removal, particle phase chemistry, and radiative properties are treated using the sectional approach. In order to keep the computational cost low, some microphysical processes are not solved in size bins where their impact is negligible (for instance sedimentation is not computed for the smallest particles).

In the setup used here, sea salt is not included in the insoluble aerosol population, and only sulphate and organic carbon are included in the smallest three size bins, which cover the nucleation mode sizes. SALSA can easily be extended to include more chemical species. An explicit kinetic solver for gas-to-particle phase partitioning has been implemented, which can, for instance, be used to model the formation of secondary organic aerosol. A detailed description of the treatment of aerosol size distribution, chemical compounds, and aerosol processes can be found in Kokkola et al. (in preparation).

HAM can be run either with or without the detailed gas-phase chemistry scheme of MOZ. If run without, then climatological fields from MOZ are used to prescribe monthly mean mixing ratios of oxidants, i.e. ozone, OH, H_2O_2, NO_2, and NO_3. If run interactively, the surface areas of HAM aerosols are used as input for the calculation of heterogeneous reaction rates (Stadtler et al., 2017). At present there is no interaction of aerosols with gas-species photolysis (MOZ uses a climatology of aerosols and lookup tables). These interactions were found to be negligible in an earlier study (Pozzoli et al., 2008a).

2.3 MOZ1.0

The Jülich Atmospheric Mechanism (JAM) version 2, which forms the basis of MOZ1.0, has its foundation in a blend of the stratospheric chemistry scheme of the Whole Atmosphere Chemistry Climate Model (WACCM; Kinnison et al., 2007), and the tropospheric Model of Ozone and Related Tracers (MOZART) version 4 (Emmons et al., 2010). The combined chemistry scheme of WACCM and MOZART has been enhanced with a detailed representation of the oxidation of isoprene following the Mainz Isoprene Mechanism 2 (MIM-2; Taraborrelli et al., 2009), and by adding a few primary volatile organic compounds and their oxidation chains. The isoprene oxidation scheme includes recent discoveries of 1,6 H-shift reactions (Peeters et al., 2009), the formation of epoxide (Paulot et al., 2009) and the photolysis of HPALD (Wolfe et al., 2012). Some of the reaction products and rates were taken from the Master Chemical Mechanism version 3.3.1 (Jenkin et al., 2015). Where no specific

Geosci. Model Dev. Discuss., https://doi.org/10.5194/gmd-2017-191
Manuscript under review for journal Geosci. Model Dev.
Discussion started: 3 November 2017

reference is provided, the reactions and reaction rate coefficients have been adopted from earlier MOZART model versions. A list of chemical species that are contained in JAM2, and the complete list of reactions can be found in the supplementary material (Tables S1–S24). In total, JAM2 contains 205 species and 734 reactions, including 142 photolysis reactions.

Table 1 lists the primary volatile organic compounds together with their respective oxidants. Radical-radical reactions have been substantially revised since (Emmons et al., 2010). In contrast to the Master Chemical Mechanism MOZART and JAM2 do not use a radical pool, but instead follow the pathways of peroxy radical reactions with HO_2, CH_3O_2, and CH_3COO_2 (peroxy acetyl) as explicitly as possible. Inorganic tropospheric chemistry considers ozone, NO, NO_2, NO_3, N_2O_5, HONO, HNO_3, HO_2NO_2, HCN, CO, H_2, OH, HO_2, H_2O_2, NH_3, chlorine and bromine species, SO_2, and oxygen atoms.

Six heterogeneous reactions are considered in the troposphere. These are: 1) uptake of ozone on dust, including the formation of HO_2; 2) uptake of HO_2 on aqueous aerosol including cloud droplets, yielding H_2O_2; 3) uptake of NO_3; 4) uptake of NO_2; 5) uptake of HNO_3 on sea salt and dust; and 6) uptake of N_2O_5. Details on the heterogeneous reactions in ECHAM-HAMMOZ and a discussion of their relevance are given in Stadtler et al. (2017).

The stratospheric chemistry scheme explicitly treats oxidation and photolysis of 21 halogenated compounds listed in Table 2 together with their approximate lifetimes. Heterogeneous reactions occur on four types of particles: 1) liquid binary sulfate (LBS); 2) supercooled ternary solution (STS); 3) nitric acid tri-hydrate (NAT); and 4) water-ice. For details, see supplement of Kinnison et al. (2007).

MOZ uses the same chemical preprocessor as CAM-Chem (Lamarque et al., 2012) and WACCM (Kinnison et al., 2007) to generate FORTRAN code which contains the chemical solver for a specific chemical mechanism. In ECHAM-HAMMOZ, all reactions are treated with the semi-implicit (Euler backward integration) solver. This solver uses efficient sparse matrix techniques (LU decomposition and Newton Raphson iteration) and is set-up as follows: within the outer timestep loop, up to 11 iterations are performed to achieve a solution within the prescribed relative accuracy. For ozone, NO, NO_2, NO_3, HNO_3, HO_2NO_2, N_2O_5, OH, and HO_2, a relative error of less than 10^{-4} is required and less than 10^{-3} for all other species. If convergence is not reached after 11 iterations, the time step is halved and the calculation is repeated. This may happen up to 5-times. If convergence is still not achieved then, a warning message is written into the log file, and the calculation continues. A three day test simulation with detailed diagnostics on the solver behaviour showed no cases where the timestep length had to be reduced, and convergence was always reached after 2 to 6 iterations. As expected, the largest number of iterations occured under conditions of sunrise and sunset. The model is parallelized in a way that blocks of entire vertical columns on several adjacent longitudes are passed to the solver together, and the convergence threshold is evaluated for the entire block for efficiency reasons. This implies that changing the vector length of the parallelisation will affect the results of the chemical calculations (within the error limits given above). More details on the MOZ chemical solver can be found in the supplementary material of Kinnison et al. (2007).

The preprocessor code is available with the ECHAM-HAMMOZ model distribution. A simplified chemistry scheme for stratospheric applications (GEOMAR Atmospheric Mechanism; GAM) is also available and can easily be used in lieu of the extensive JAM2 mechanism (Wahl et al., in preparation).

Geosci. Model Dev. Discuss., https://doi.org/10.5194/gmd-2017-191
Manuscript under review for journal Geosci. Model Dev.
Discussion started: 3 November 2017

Geoscientific Model Development Discussions
Open Access
EGU

Table 1. Primary volatile organic compounds and their oxidants in the JAM2 mechanism. BIGALKANE is a lumped species for all alkanes C_4 and greater, BIGENE lumps all alkenes C_4 and greater. o-, m-, and p-xylene are lumped into one xylene species. CH_4 is also oxidzed by O(1D) and F, CH_2O is also oxidized by O and HO_2, DMS is also oxidized by BrO, CH3Br and HCN are also oxidized by O1D.

Species	Long name	OH	O_3	NO_3	Cl	Br
CH_4	methane	yes	no	no	yes	no
C_2H_6	ethane	yes	no	no	yes	no
C_3H_8	propane	yes	no	no	yes	no
BIGALKANE	alkanes $\geq$ C4	yes	no	no	yes	no
C_2H_2	acetylene	yes	no	no	yes	no
C_2H_4	ethene	yes	yes	no	yes	no
C_3H_6	propene	yes	yes	yes	no	no
BIGENE	alkenes $\geq$ C4	yes	no	no	no	no
C_5H_8	2-methylbuta-1,3-diene (isoprene)	yes	yes	yes	no	no
APIN	α-pinene	yes	yes	yes	no	no
BPIN	β-pinene	yes	yes	yes	no	no
LIMON	limonene	yes	yes	yes	no	no
MYRC	myrcene	yes	yes	yes	no	no
BCARY	β-caryophyllene	yes	yes	yes	no	no
BENZ	benzene	yes	no	no	no	no
TOL	toluene	yes	no	no	no	no
XYL	xylenes	yes	no	no	no	no
CH_3OH	methanol	yes	no	no	yes	no
C_2H_5OH	ethanol	yes	no	no	no	no
PHENOL	phenol	yes	no	yes	no	no
MBO	2-methylbut-3-en-2-ol	yes	yes	yes	no	no
CH_2O	formaldehyde	yes	no	yes	yes	yes
CH_3CHO	acetaldehyde	yes	no	yes	yes	yes
BZALD	benzaldehyde	yes	no	no	no	no
CH_3COCH_3	acetone	yes	no	no	yes	no
MEK	butan-2-one	yes	no	no	yes	no
HCOOH	formic acid	yes	no	no	no	no
CH_3COOH	acetic acid	yes	no	no	yes	no
DMS	dimethyl sulfide	yes	no	yes	yes	yes
CH_3BR	methyl bromide	yes	no	no	yes	no
CH_3CL	methyl chloride	yes	no	no	yes	no
CH_3CN	methyl cyanide	yes	no	no	yes	no

Geosci. Model Dev. Discuss., https://doi.org/10.5194/gmd-2017-191
Manuscript under review for journal Geosci. Model Dev.
Discussion started: 3 November 2017

Geoscientific Model Development Discussions

Table 2. Halogenated compounds in JAM2 with relevance for stratospheric ozone chemistry and their approximate lifetimes in years (Miller et al., 1998; Liang et al., 2010; WMO, 2014; Harrison et al., 2016).

Species	Long name	Approximate lifetime
$CHBR_3$	bromoform	0.055 (40 days)
CH_2BR_2	dibromomethane	0.38 (140 days)
CH_3BR	methyl bromide	0.8
CH_3CL	methyl chloride	0.9
H1202	Halon-1202 (CBr_2F_2)	2.5
CH_3CCL_3	methyl chloroform	5.0
HCFC141B	HCFC-141b (CH_3CCl_2F)	9.4
HCFC22	HCFC-22 ($CHClF_2$)	10
CF_2CLBR	Halon-1211	16
HCFC142B	HCFC-142b (CH_3CClF_2)	18
CCL_4	Carbon tetrachloride	26
H2402	Halon-2402 ($CBrF_2CBrF_2$)	28
CFC11	CFC-11 (CCl_3F)	52
CF3BR	Halon-1301	72
CFC113	CFC-113 (CCl_2FCClF_2)	93
CFC12	CFC-12 (CCl_2F_2)	102
CFC114	CFC-114 ($CClF_2CClF_2$)	189
CFC115	CFC-115 ($CClF_2CF_3$)	540
SF_6	sulfurhexafluoride	3200

3 Chemical parametrizations

3.1 Emissions

All emissions in the ECHAM-HAMMOZ model are controlled via a single "emi_spec" file which provides a simple and compact way to define all trace gas and aerosol emissions used in a model simulation and ensures proper documentation of the emissions used in a specific run. The emi_spec file consists of three sections: 1) definition of emission sectors and the source of emission information for this sector; 2) the species-sector matrix controlling which emission sectors are active for which species; and 3) an alias table that allows the mapping of species names from emission files to the names that are defined in the chemical mechanism. The emi_spec file that was used in the simulations of this paper is provided in supplement 2.

In the sector definition, users can specify if emissions from that sector shall be read from file, or if an interactive parametrization (if available) shall be applied. In addition, it is possible to specify a single number to be used as a globally uniform emission mass flux. Furthermore, it can be decided to apply the emissions as a boundary flux condition to the lowest model level, to inject them at the model level near 50 m altitude (smoke stack emissions), or to distribute them within a specific range of

Geosci. Model Dev. Discuss., https://doi.org/10.5194/gmd-2017-191
Manuscript under review for journal Geosci. Model Dev.
Discussion started: 3 November 2017

the atmosphere. For biomass burning emissions a special option is available to distribute them across the planetary boundary layer. Finally, the user can also select if emissions shall be interpolated in time or not, and if the year of the date information in an emissions file shall be ignored in order to treat emissions as a climatology. The simulations shown in this article were performed without time interpolation (i.e. applying monthly step changes) and using emissions for specific years.

The species-sector matrix has a single float number or a dash in each cell. The float number can be used to easily scale emissions from a particular sector for a particular species, or to define emissions for compounds for which no emission data are available by scaling these emissions to those of other compounds (this requires an entry in the alias table). A dash indicates that no emissions for this compound are available in the given sector and is distinct from a zero, which would attempt to read or calculate emissions and then scale them to zero afterwards.

Emission files can be provided in any time resolution (minimum daily). Normally, all emissions files contain monthly data, except for fire emissions, which are provided in daily resolution in the standard configuration.

With JAM2 and either HAM-M7 or HAM-SALSA as aerosol module, ECHAM-HAMMOZ has emissions for a total of 43 species that are emitted in 20 sectors. Table 3 lists all emissions for the year 2008.

In the standard configuration of ECHAM-HAMMOZ, the following emissions are calculated interactively: 1) VOC emissions from terrestrial vegetation (MEGAN; Guenther et al., 2012 ; implementation details in Henrot et al., 2017); 2) DMS emissions from the oceans (Kloster et al., 2006; Lana et al., 2011); 3) dust (Stier et al., 2005); 4) sea salt (Guelle et al., 2001); 5) volcanic sulfur (Dentener et al., 2006b). Emissions from agriculture (AGR) and waste burning (AWB), forest fires (FFIRE) and grassland fires (GFIRE), aircraft (AIRC), domestic fuel use (DOM), energy generation, including fossil fuel extraction (ENE), industry (IND), ship traffic (SHP), solvent use (SLV), transportation (TRA), and waste management (WST) are taken from the Atmospheric Chemistry Climate Model Intercomparison Project (ACCMIP; Lamarque et al., 2010). More specifically, as the simulations described here focus on the period after 2000, we make use of the Representative Concentration Pathway (RCP) 8.5 emissions (van Vuuren et al., 2011). The original files, which had a temporal resolution of 10 years, were interpolated to individual years and seasonal cycles were added (Granier et al., 2011). The netCDF emission data files are available from a WebDAV server at the Forschungszentrum Jülich (http://accmip-emis.iek.fz-juelich.de/) and contain detailed README and metadata information.

Ocean emissions of reactive VOC were obtained from the POET project (Granier et al., 2005), and terrestrial DMS emissions are from (Dentener et al., 2006b).

3.2 Lightning

As described in Rast et al. (2014), lightning NO_x emissions are parameterized as a function of the average convective updraft velocity $\overline{w}$ in a model column following Grewe et al. (2001). Flash frequency is calculated as

$$F = a(\overline{w}/\overline{w}_0\sqrt{d/d_0})^{\beta}, \quad (1)$$

Geosci. Model Dev. Discuss., https://doi.org/10.5194/gmd-2017-191
Manuscript under review for journal Geosci. Model Dev.
Discussion started: 3 November 2017

Geoscientific Model Development Discussions
Open Access
EGU

Table 3. Emissions of trace gases and aerosols used in the standard configuration of ECHAM-HAMMOZ for the year 2008.

Species	Long name	Emissions in Tg(species)
APIN	α-pinene	27.173
BC	black carbon	7.847
BCARY	β-caryophyllene	3.941
BENZ	benzene	9.262
BIGALKANE	alkanes $\geq$ C4	45.650
BIGENE	alkenes $\geq$ C4	14.120
BPIN	β-pinene	16.123
BZALD	benzaldehyde	0.027
C_2H_2	acetylene	4.732
C_2H_4	ethene	38.628
C_2H_5OH	ethanol	17.510
C_2H_6	ethane	15.392
C_3H_6	propene	21.761
C_3H_8	propane	7.181
C_5H_8	isoprene	442.094
CH_2O	formaldehyde	12.581
CH_3CHO	acetaldehyde	20.890
CH_3CN	acetonitrile	2.763
CH_3COCH_3	acetone	37.316
CH_3COOH	acetic acid	29.343
CH_3OH	methanol	121.335
CH_4	methane	358.188
CO	carbon monoxide	1129.770
DMS	dimethylsulfide	51.530
DU	dust	1140.523
H_2	hydrogen	27.762
HCN	hydrogen cyanide	5.051
HCOOH	formic acid	7.589
LIMON	limonene	8.558
MBO	methyl butenol	2.053
MEK	butan-2-one	3.612
MYRC	myrcene	2.394
NH_3	ammonia	52.065
NO	nitrogen monoxide	94.547
NO_2	nitrogen dioxide	4.896
OC	organic carbon	49.589
PHENOL	phenol	1.359
SO_2	sulfur dioxide	132.636
SO_4	sulfate	5.100
SS	sea salt	5608.551
TOL	toluene	10.117
XYL	xylene(s)	13.136

Geosci. Model Dev. Discuss., https://doi.org/10.5194/gmd-2017-191
Manuscript under review for journal Geosci. Model Dev.
Discussion started: 3 November 2017

Geoscientific Model Development Discussions

with $a = 1.54 \times 10^{-5}$, $\beta = 4.9$, $\overline{w}_0 = 1\,\mathrm{m/s}$, $d_0 = 1\,\mathrm{m}$. d is the vertical cloud extent. Due to the coarse model resolution, a correction factor of 0.7 is applied to the result of this formula to yield a global flash frequency of 49 flashes per second for the year 2008, which is within the uncertainty of 44 ± 5 flashes per second observed from the Optical Transient Detector satellite instrument during 1995 to 2000 (Christian et al., 2003).

The fraction of cloud-to-ground flashes is calculated according to Price and Rind (1994) as

$$f_{cg} = (0.021 d_c^4 - 0.648 d_c^3 + 7.49 d_c^2 - 36.54 d_c)^{-1}. \quad (2)$$

d_c denotes the cold cloud thickness, i.e. the vertical extent of the part of the cloud with temperatures below freezing. Following Price et al. (1997) the amount of NO generated per flash is given as $1 \times 10^{17} \mathrm{molec.\,J^{-1}}$, and average flash energies are assumed to be 6.7×10^9 J for cloud-to-ground flashes, and one tenth of this for intra- and inter-cloud flashes. With these factors applied, the global amount of NO generated from lightning in the year 2008 would be 5.05 $\mathrm{Tg(N)}$, which is well within range of other estimates (e.g. Schumann and Huntrieser, 2007) and was recommended as a target value in earlier model intercomparison projects. Recent modeling studies tend to adopt lower global lightning $\mathrm{NO_x}$ emissions. As we found a significant influence of global lightning $\mathrm{NO_x}$ on global tropospheric ozone and OH (see section 6) with methane and methylchloroform lifetimes more within the range of literature values at lower lightning $\mathrm{NO_x}$, we scaled the lightning emissions down. In the default configuration of the model, global lightning $\mathrm{NO_x}$ emissions from the simulation described in this study for the year 2008 are 1.2 $\mathrm{Tg(N)}$. Within the model column, the NO from lightning is distributed according to the climatological vertical profiles of Pickering et al. (1998).

3.3 Lower boundary conditions for long-lived stratospheric species

Halogenated species which are primarily decomposed in the stratosphere are not emitted into the model, but instead a lower boundary condition is specified for these compounds. In addition to the species in Table 2 the model also specifies lower boundary conditions for $\mathrm{N_2O}$, $\mathrm{CH_4}$, and $\mathrm{CO_2}$. The latter can be turned off if the model is run with all carbon cycle components. The lower boundary conditions are provided as zonally averaged, monthly values from the Whole Atmosphere Chemistry Climate Model (WACCM) input for the simulations in the Chemistry Climate Modelling Initiative (CCMI) initiative (cf. section 2.3.2 in Tilmes et al., 2016). The organic halogen scenario (here, RCP8.5) is based on WMO (2011) and described in Eyring et al. (2013), and Morgenstern et al. (2017). Boundary conditions for $\mathrm{N_2O}$, $\mathrm{CH_4}$, and $\mathrm{CO_2}$ are taken from Meinshausen et al. (2011) as recommended by CCMI. As described in Tilmes et al. (2016), the boundary conditions used in ECHAM-HAMMOZ include a latitudinal gradient based on aircraft measurements from the HIAPER (High-Performance Instrumented Airborne Platform for Environmental Research) Pole-to-Pole Observations (HIPPO) campaigns (Wofsy et al., 2011).

The lower boundary condition for methane uses a relaxation to the climatological values with an e-folding time of 3 days in order to preserve regional methane emission patterns while at the same time preventing a drift of methane concentrations due to possibly unbalanced sources and sinks (cf. Rast et al., 2014).

Geosci. Model Dev. Discuss., https://doi.org/10.5194/gmd-2017-191
Manuscript under review for journal Geosci. Model Dev.
Discussion started: 3 November 2017

3.4 Photolysis

As described in the supplement of Kinnison et al. (2007), photolysis frequencies are calculated as a product of the prescribed extra-atmospheric solar flux, the atmospheric transmission function (dependent on model calculated ozone and O_2), the molecular absorption cross section, and the quantum yield of the specific reaction channel. There are 34 channels in the wavelength regime from 120 to 200 nm, and 122 channels between 200 and 750 nm. At wavelengths less than 200 nm, the transmission function is computed explicitly, and absorption cross sections and quantum yields are prescribed, except for O_2 and NO, where detailed parameterizations are used (see supplement of Kinnison et al., 2007). Beyond 200 nm, the transmission function is calculated from a lookup table as a function of altitude, column ozone, surface albedo, and zenith angle. The maximum zenith angle for which photolysis frequencies are calculated is 97°. The temperature and pressure dependence of absorption cross sections and quantum yields is also interpolated from lookup tables.

The UV albedo is parameterized according to Laepple et al. (2005) using satellite-derived albedo maps for snow and non snow conditions based on the Moderate Resolution Imaging Spectroradiometer (MODIS) instrument. The threshold for switching from non snow to snow values is a snow depth of 1 cm calculated by ECHAM. Sea ice albedo is prescribed as 0.78 in the Northern hemisphere, and 0.89 in the Southern hemisphere, respectively. The albedo over ice-free oceans is set to 0.07. The influence of clouds is parameterized according to Brasseur et al. (1998) through computation of an effective albedo and modification of the atmospheric transmission function. Both effects are combined into a single factor that varies by model level.

3.5 Dry deposition

Deposition of trace gases and aerosols on the Earth surface is parameterized according to the resistance model of Wesely (1989) using a big-leaf approach for vegetated surfaces (Ganzeveld and Lelieveld, 1995). The ECHAM-HAMMOZ dry deposition scheme distinguishes between vegetated land surfaces, bare soils, water, and snow/ice and uses the corresponding surface types from the JSBACH land model (see section 2.1).

As described in Stier et al. (2005), the leaf area index is taken from a NDVI (Normalised Differential Vegetation Index) climatology (Gutman et al., 1995) and the Olson (1992) ecosystem database. Canopy height, roughness length, and forest fraction are from a climatology. Soil pH is specified for 11 different soil types. Technically, these parameters can also be obtained online from the JSBACH land surface model. This has been tested in Stanelle et al. (2014).

Surface resistances are explicitly specified for H_2SO_4, HNO_3, NO, NO_2, O_3, and SO_2. Those of other species are calculated relative to O_3 and SO_2 following Wesely (1989). Henry coefficients and reactivity factors have been defined for 135 species (see Table S25 in supplement 1). All of these species can be deposited, however, for most of them the deposition rates will be very small due to low Henry values or low reactivities. Where available, Henry coefficients were taken from the literature, in other cases we assumed that molecules with similar structures have Henry values on the same order of magnitude. In particular, OOH groups were considered similar to OH groups in terms of their impact on Henry constants. Organic peroxides (ROOH) are assumed to have a surface reactivity f_0 of 1. Other organic molecules with oxygen were assigned with f_0 = 0.1. Note that

Geosci. Model Dev. Discuss., https://doi.org/10.5194/gmd-2017-191
Manuscript under review for journal Geosci. Model Dev.
Discussion started: 3 November 2017

while HO_2 can undergo dry deposition ($H = 690\,M\,atm^{-1}$), we did not define Henry values and surface reactivities for organic peroxy radicals, although some of these (notably from higher oxidation states) might well be soluble and could therefore be efficiently removed by dry deposition.

3.6 Wet deposition and scavenging

The ECHAM-HAMMOZ wet deposition scheme is based on Croft et al. (2009) for below-cloud scavenging by rain and snow and Croft et al. (2010) for in-cloud (nucleation and impaction) scavenging. The in-cloud scavenging scheme treats nucleation and impact scavenging in stratiform and convective clouds and distinguishes between warm, cold, and mixed-phase clouds. For aerosols, scavenging also takes place below clouds in rain and snow. For gases, the fraction dissolved in the liquid phase is calculated based on Henry's law (see Table S25), and no below-cloud scavenging takes place except for HNO_3 and H_2SO_4.

4 Simulation set-up

The simulations described in this article are based on the ECHAM-HAMMOZ model version and input data sets as released in February 2017. The reference run is a 10-year simulation from October 2002 through December 2012 (the first three months are used as spin-up time and are not used in the analysis). It uses the HAM-SALSA aerosol scheme for aerosol formation and microphysical processes. The simulation includes full interaction between aerosols and gas-phase chemistry, aerosol and clouds, full feedback of aerosols and trace gases on the radiation, and feedback of chemically produced water in the stratosphere onto the climate model. The model resolution is $1.875° \times 1.875°$ in longitude and latitude (spectral triangular truncation T63), and 47 vertical levels from the surface to 0.01 hPa (full level pressure). The corresponding model time step is 7.5 minutes. Sea-surface temperatures and sea-ice coverage are prescribed for each year of simulation, following the Coupled Model Intercomparison Project Phase 5 (CMIP5) AMIP-simulation protocol (Giorgetta et al., 2012) and using the data from the PCMDI CMIP archive (PCMDI, 2017). In addition, temperature, vorticity, divergence, and surface pressure from 6-hourly output of the European Centre for Medium Range Weather Forecast (ECMWF) ERA-Interim reanalysis (Dee et al., 2011) were used to specify the dynamics of "real weather" in nudging mode (Kaas et al., 2000).

The analyses presented below focus on the year 2008. This year was chosen as a reference year by the HAMMOZ consortium, because of data availability and because it has been used in several other studies and in the Copernicus Atmospheric Monitoring Service validation activities (Eskes et al., 2015).

As described above, the released model version has very low lightning NO emissions, and the parameterisation of the heterogeneous reaction of HNO_3 neglects the potential of re-evaporation of aerosol nitrate to gaseous HNO_3 (Stadtler et al., 2017), which has an impact on the total amount of deposited nitrogen and also affects the budgets of ozone and nitrogen oxides as shown below. In order to investigate the impacts of these two factors we performed a small series of sensitivity simulations for the year 2008, based on restart files of the reference run. Table 4 briefly describes these simulations. Two of the simulations double and quadruple the amount of lightning emissions, respectively, so that they are more in line with

Geosci. Model Dev. Discuss., https://doi.org/10.5194/gmd-2017-191
Manuscript under review for journal Geosci. Model Dev.
Discussion started: 3 November 2017

Geoscientific Model Development Discussions

Table 4. Summary of simulations performed for the analysis of global trace gas budgets in this article.

Name	Period	Lightning	Description
reference	2003-2012	1.2 $\mathrm{Tg(N)}$	reference run as released
lght*2	2008	2.4 $\mathrm{Tg(N)}$	as reference run but with doubled lightning emissions
lght*4	2008	4.8 $\mathrm{Tg(N)}$	as reference run but with quadrupled lightning emissions
no_het_$\mathrm{HNO_3}$	2008	1.2 $\mathrm{Tg(N)}$	as reference run but without the heterogeneous loss reaction of $\mathrm{HNO_3}$

current estimates ranging from 2 to 8 $\mathrm{Tg(N)\,yr^{-1}}$ (Schumann and Huntrieser, 2007). The other simulation de-activates the heterogeneous reaction of $\mathrm{HNO_3}$ on seasalt and dust and is otherwise identical to the reference run.

5 Comparison with observations

5.1 Total column ozone and stratospheric processes

We begin our model evaluation with a discussion of seasonal total column ozone (TCO) distributions in comparison with retrievals from the Infrared Atmospheric Sounding Interferometer (IASI), onboard the sun-synchronous polar-orbiting MetOp platforms, and from the Ozone Monitoring Instrument (OMI) onboard the Aura satellite (Levelt et al., 2006).

IASI is a Fourier Transform Spectrometer designed to measure the outgoing infrared radiation from the Earth's surface and the atmosphere in a nadir-viewing geometry (Clerbaux et al., 2009). The first IASI instrument was launched in 2006 on the MetOp-A platform and it is still operating. A second instrument onboard MetOp-B was launched in 2012. IASI measures the thermal infrared emission between 645 to 2760 $\mathrm{cm^{-1}}$ (15.5 and 3.62 µm) with a spectral resolution of 0.5 $\mathrm{cm^{-1}}$ after apodization. For a reference blackbody at 280 K, the wavenumber-dependent radiometric noise varies between 0.1 and 0.3 K below 2250 $\mathrm{cm^{-1}}$. IASI observations – a set of four simultaneous footprints of 12 km at nadir – are performed every 50 km along the track of the satellite at nadir and across-track over a swath width of 2200 km. The high spectral resolution and low radiometric noise allow the retrieval of numerous gas-phase atmospheric species (e.g. Clerbaux et al., 2009; Hilton et al., 2012). IASI crosses the equator at around 09:30 and 21:30 mean local solar time, achieving near global coverage twice a day.

Vertical abundance and distribution of three species, namely $\mathrm{O_3}$, CO and $\mathrm{HNO_3}$, are retrieved in near real-time from individual IASI measurements with the Fast Optimal Retrievals on Layers for IASI (FORLI) algorithm. Fully described in Hurtmans et al. (2012), FORLI is based on a fast radiative transfer code and implements the optimal estimation method (Rodgers, 2000) for solving the ill-posed inversion problem. Prior to the inversion process, IASI observations are filtered out according to the cloud coverage and the Level 2 availability. The individual retrievals also undergo several quality controls to ensure stable and consistent products. All details as to the retrieval methodology, characterization of the retrieved products and validation against a large suite of independent ground-based, airborne and satellite measurements can be found in Boynard et al. (2016) and in Wespes et al. (2016, 2017) for $\mathrm{O_3}$, in George et al. (2015) for CO, and in Ronsmans et al. (2016) for $\mathrm{HNO_3}$.

Geosci. Model Dev. Discuss., https://doi.org/10.5194/gmd-2017-191
Manuscript under review for journal Geosci. Model Dev.
Discussion started: 3 November 2017

Geoscientific Model Development Discussions

The estimated errors on the retrieved total columns are mainly latitude-dependent. For O_3, such errors are usually below 3 %, but slightly larger (7.5 % on average) when the signal is particularly weak over the Antarctic ozone hole or due to strong water vapour influence at tropical latitudes (Hurtmans et al., 2012). The error on the retrieved CO total columns is generally below 10-15 % at mid- and tropical latitudes, but increases up to 20-25 % in polar regions (George et al., 2015).

Figure 1 compares seasonal mean total ozone columns of the year 2008 from the ECHAM-HAMMOZ reference simulation with IASI retrievals. The model generally captures the highs and lows that are observed by the satellite as well as the changes of these patterns throughout the seasons. It has a tendency to underestimate the IASI observations of TCO by up to -30 DU in high Northern latitudes during winter and spring, and over the Antarctic in all seasons, but the deviations are generally within the error limits of the retrievals.

OMI is an ultraviolet/visible nadir viewing solar backscatter spectrometer. We use the level 3 data product which is globally gridded to 1°latitude by 1°longitude. The Aura OMI data spans the temporal range from 2004 to present. Daily OMI data are interpolated to the model resolution and compared to the model results as latitude-timeseries plots in Figure 2. Overall the global representation of the model and OMI observations of TCO are in excellent agreement. This is especially true for the representation of the heterogeneous chemistry defining the Antarctic ozone hole (see Solomon, 1999, and references within). Here, the ECHAM-HAMMOZ model accurately represents the distribution of Antarctic springtime TCO. However, careful examination shows a model bias of up to +20 DU compared to OMI, whereas the model TCO show an overall negative bias to IASI (Figure 1). Both, the apparent model underestimation with respect to IASI and the overestimation with respect to OMI, are within the uncertainties of the retrievals. Systematic biases can be explained by different sampling patterns and measurement principles (for example, IASI as an infrared sensor measures during daytime and nighttime, while UV and visible sensors are limited to daytime observations), and to differences in the weighting functions and retrieval algorithms. IASI TCO have been found to be larger by 10–11 % compared to TCO from another UV-vis satellite sensor, the Global Ozone Monitoring Experiment-2 (GOME-2) instrument, and from ground-based UV Brewer-Dobson data (Boynard et al., 2016).

Figure 3 further explores the representation of the Antarctic region by showing a time-dependent vertical cross section of key constituents at 81°S. In this figure, model results of temperature, nitric acid (HNO_3), chlorine monoxide (ClO), and ozone are compared to daily binned (4.5°latitude × 10 °longitude) data from Version 4 of the Microwave Limb Sounder (MLS) instrument onboard the Aura satellite. Details of the accuracy and precision of the MLS observations are discussed in (Livesey et al., 2016). Since polar heterogeneous chemistry is very temperature sensitive (e.g. Solomon et al., 2015)) it is important to have an accurate representation of temperature when comparing model results to observational data for a given year. Figure 3, row 1 shows excellent agreement between the retrieved MLS temperatures and those used in ECHAM-HAMMOZ giving confidence that there are no model temperature biases that could impact the heterogeneous chemistry derived in the model. Another important constituent to show is HNO_3. Here, the HNO_3 gas-phase abundance is affected by formation of NAT PSC particles which can settle out of the stratosphere and cause irreversible denitrification. Figure 3, row 2 shows that the model does an adequate job of representing the HNO_3 abundance and the process that controls loss of total inorganic nitrogen in the model atmosphere; if anything, the model over denitrifies by 0.5 ppbv. This result is consistent with use of the current

Geosci. Model Dev. Discuss., https://doi.org/10.5194/gmd-2017-191
Manuscript under review for journal Geosci. Model Dev.
Discussion started: 3 November 2017

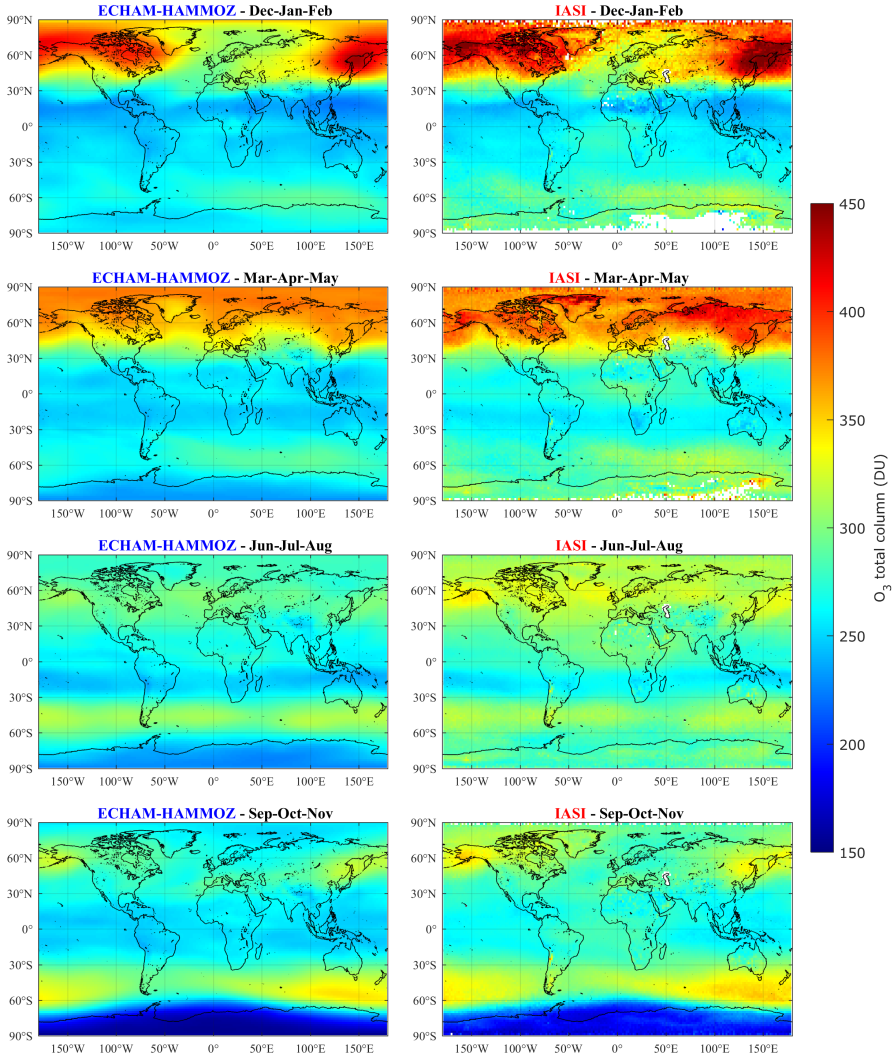

Figure 1. Comparison of seasonal mean total column ozone (in DU) by ECHAM-HAMMOZ with data from the IASI instrument. Data and model results are from 2008; IASI data were interpolated to the model grid.

ECHAM-HAMMOZ heterogeneous chemistry module (Kinnison et al., 2007) in other model frameworks, e.g., the Whole Atmosphere Chemistry Climate Model, version 3 (see evaluation in SPARC, 2010).

The chlorine monoxide distribution is shown in Figure 3, row 3. The overall gas-phase chemistry that controls ClO abundance in the upper stratosphere and the heterogeneous chemistry activation of halogens on PSCs in the lower stratospheric is consistent between model and observations. However, a close examination shows differences in the vertical extent, magnitude, and timing of the ClO abundance in the model compared to observations. These differences will be explored in future work. The ozone evolution is shown in Figure 3, row 4. The overall representation of ozone from the lower mesosphere to the lower

Geosci. Model Dev. Discuss., https://doi.org/10.5194/gmd-2017-191
Manuscript under review for journal Geosci. Model Dev.
Discussion started: 3 November 2017

Geoscientific Model Development Discussions

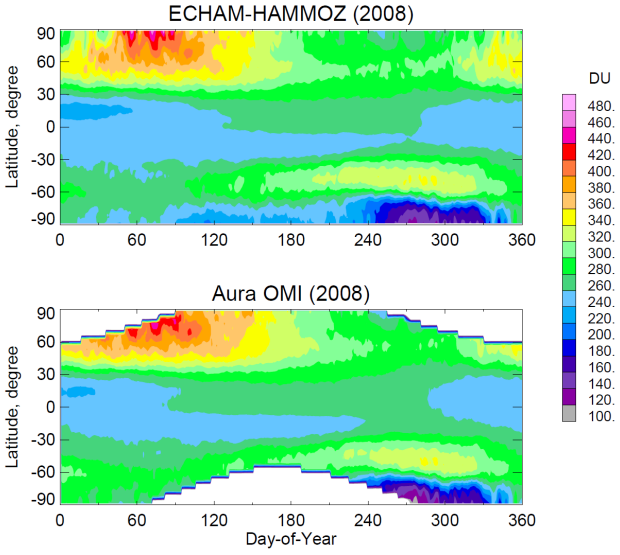

Figure 2. Comparison of the seasonal cycle of zonal mean total column ozone (in DU) between ECHAM-HAMMOZ (top panel) and Aura OMI (bottom panel). Data and model are for year 2008. Aura OMI data was interpolated to model grid.

stratosphere is captured by the model. However, in the lower stratosphere spring, the model is biased high by approximately +0.5 ppmv. This high ozone bias translates to the model having too much TCO in the Antarctic spring period, consistent with the discussion of Figure 2.

5.2 Tropospheric ozone

Figure 4 shows the annual mean bias of ozone in comparison to the ozone sonde climatology of Tilmes et al. (2012) at three different pressure levels. For ease of comparison, we have chosen a similar layout and scale as Lamarque et al. (2012) except that we display absolute differences also at 250 hPa. At 250 hPa, the biases are generally between -35 and + 35 ppbv with the exception of high Northern latitude stations, where the bias is as low as -114 ppbv (-37 %; Eureka and Resolute, Canada) and Prague, Czech Republic, where the bias is +66 ppbv (+111 %). The model overestimate at high northern latitudes is qualitatively similar to CAM-Chem (Lamarque et al., 2012). We concur with the authors of that paper that the reason is likely associated with a mismatch between the model tropopause and the real tropopause in this region. Due to the very steep gradients of ozone around the tropopause, even small vertical displacements can lead to large discrepancies of simulated ozone values if the comparison is made on pressure levels. Future work should probably consider to evaluate models with ozonesonde data relative to the tropopause.

In contrast to CAM-Chem, the northern hemisphere mid latitude biases in ECHAM-HAMMOZ are more or less equally distributed. One may discern a tendency of the model to overestimate ozone at 250 hPa around the Pacific, whereas there appears to be underestimation around the Atlantic.

Geosci. Model Dev. Discuss., https://doi.org/10.5194/gmd-2017-191
Manuscript under review for journal Geosci. Model Dev.
Discussion started: 3 November 2017

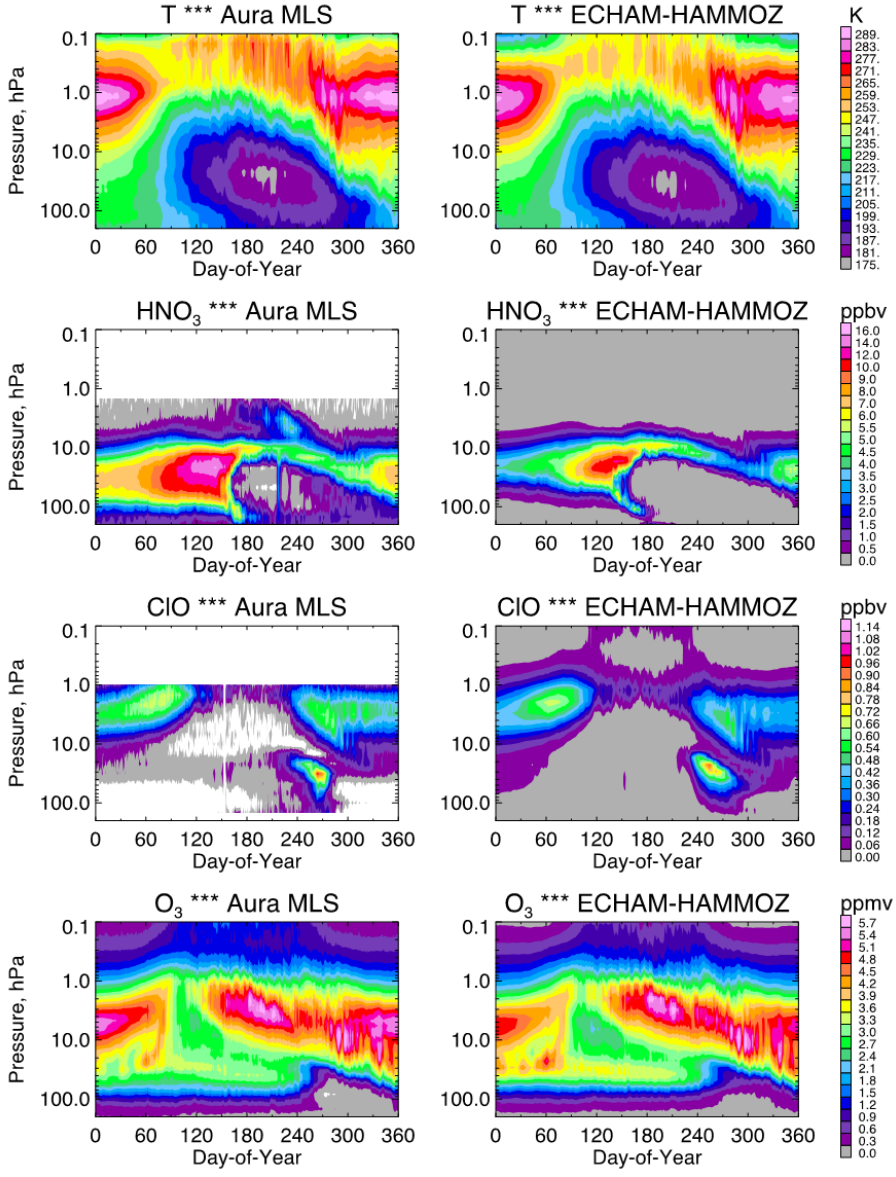

Figure 3. Comparison of temperature, HNO_3, ClO, and O_3 between Aura MLS observations (left column) and ECHAM-HAMMOZ (right column) Data and model are for year 2008.

At 500 hPa, the pattern of the ECHAM-HAMMOZ biases is similar to that at the 250 hPa level, but the values are generally smaller. Only 6 stations out of 42 have biases with absolute values larger than 10 ppbv, and 5 of these 6 stations are located in the tropics. Ascension, Natal, and Reunion exhibit large low biases, whereas high biases are found at Hilo, Hawaii, and Samoa. At 800 hPa the biases are somewhat shifted to more positive values, so that no site has a low bias of more than 10 ppbv, and

Geosci. Model Dev. Discuss., https://doi.org/10.5194/gmd-2017-191
Manuscript under review for journal Geosci. Model Dev.
Discussion started: 3 November 2017

Geoscientific Model Development Discussions
Open Access
EGU

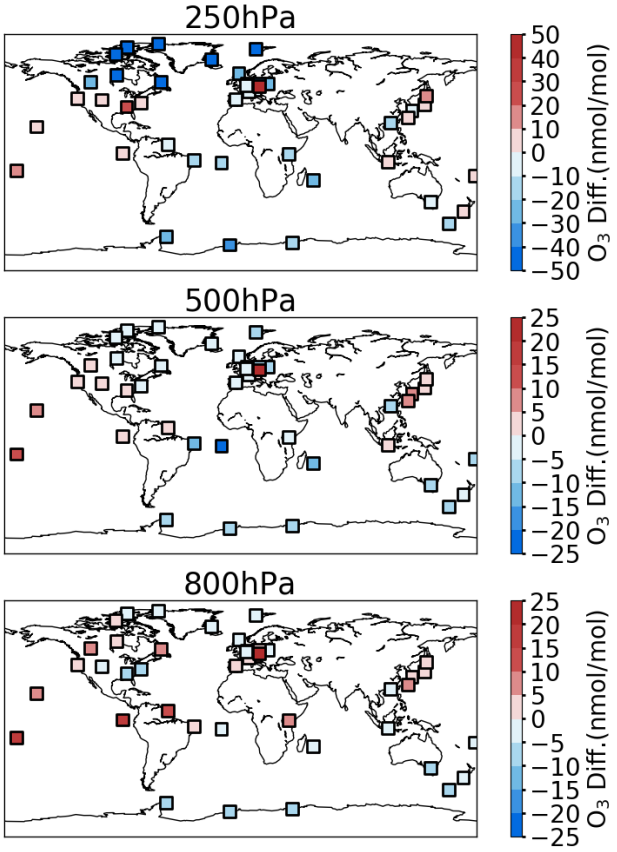

Figure 4. Annual mean bias of ECHAM-HAMMOZ with respect to ozone sonde data from Tilmes et al. (2012) at 250 hPa (top), 500 hPa (middle), and 800 hPa (bottom). Figure layout and scales are comparable to Lamarque et al. (2012), except that absolute errors are shown at 250 hPa.

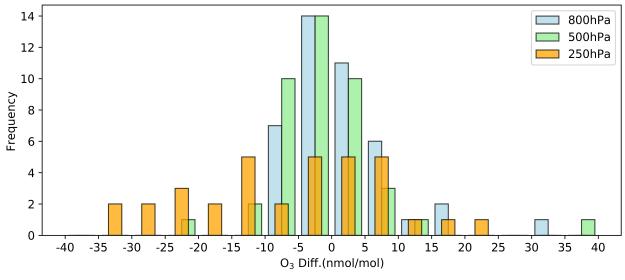

Figure 5. Frequency distributions of the ozone bias (in ppbv) at the 42 stations from Tilmes et al. (2012). Note: high northern latitude stations with biases larger than ±40ppbv at 250 hPa are not shown.

Geosci. Model Dev. Discuss., https://doi.org/10.5194/gmd-2017-191
Manuscript under review for journal Geosci. Model Dev.
Discussion started: 3 November 2017

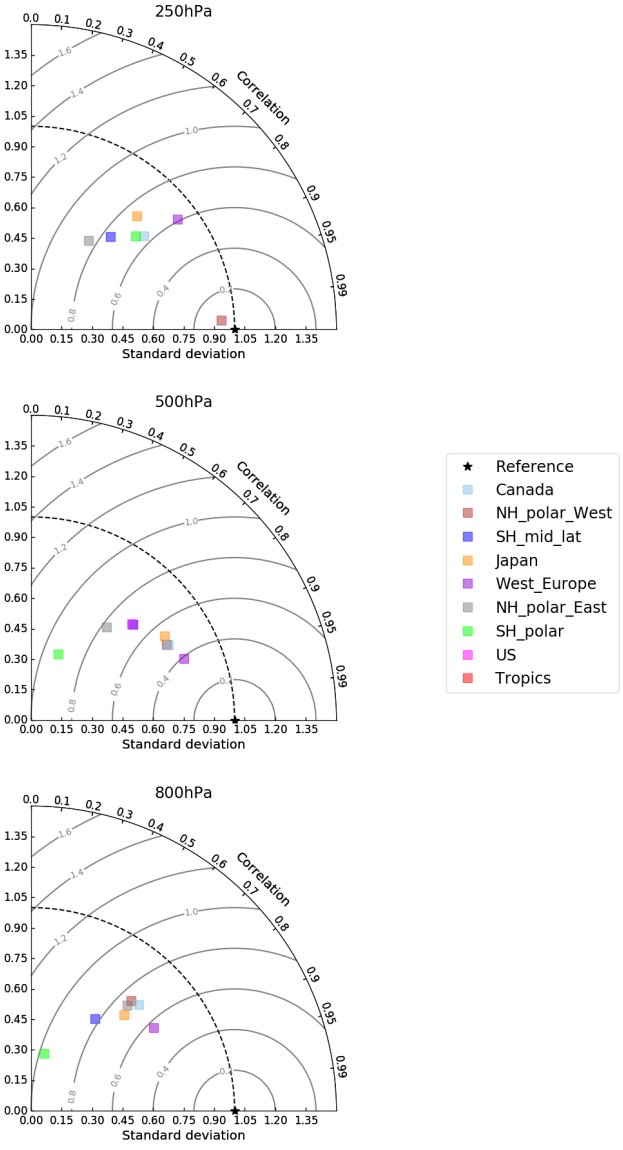

Figure 6. Taylor plots of regional averaged ozone sondes at 250 hPa (top), 500 hPa (middle), and 800 hPa (bottom). Ozone sonde data and region definitions are from Tilmes et al. (2012). Where a region is not shown in a panel, the respective data point is outside the axis range.

4 stations show a high bias greater 10 ppbv. Averaged over all 42 sites, the mean biases at 250, 500, and 800 hPa are -17.8, -1.5, and +1.6 ppbv, respectively. If we exclude the high latitude northern hemisphere stations, the bias at 250 hPa is reduced to -3.6 ppbv. Figure 5 shows frequency distributions of the model biases at the three pressure levels.

The seasonal cycle of tropospheric ozone is evaluated with help of Taylor plots in Figure 6. Similar to Lamarque et al. (2012) we show regional averages at the three pressure levels of Figure 4. However, we retain the original region definitions and color

Geosci. Model Dev. Discuss., https://doi.org/10.5194/gmd-2017-191
Manuscript under review for journal Geosci. Model Dev.
Discussion started: 3 November 2017

Geoscientific Model Development Discussions
Open Access
EGU

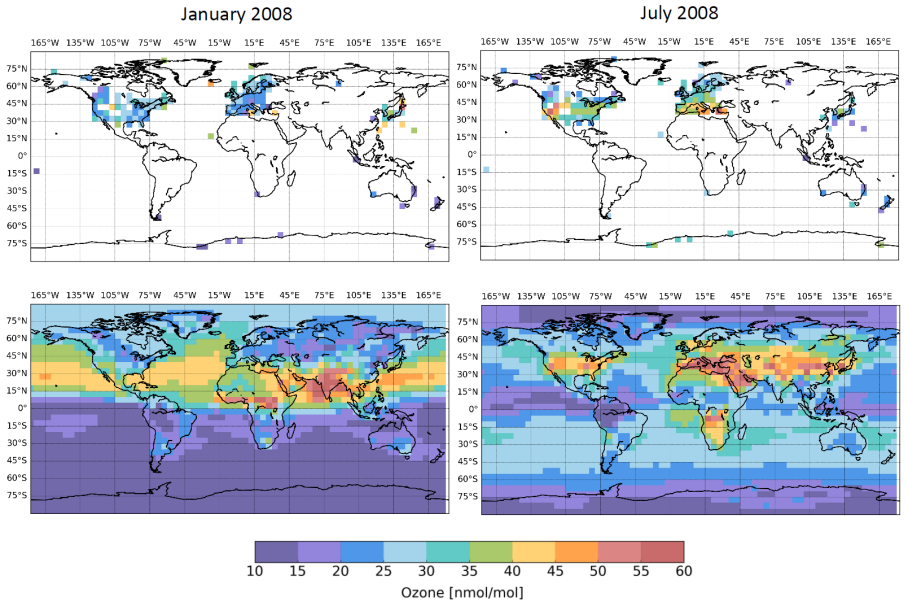

Figure 7. Comparison of gridded rural surface ozone observations from the TOAR database (Schultz et al., 2017) (top row) with ECHAM-HAMMOZ output (bottom row) for January and July 2008. The model results have been regridded to 5 °× 5 °to match the resolution of the observations.

codings of Tilmes et al. (2012). Taylor plots with individual stations and also for the sensitivity run lght*4 can be found in supplement 3. For seven out of nine regions, the correlation between the observed and simulated seasonal cycle is positive, so that the symbols appear in Figure 6. Exceptions are the US (250 and 800 hPa) and the tropics. The normalized root mean square error (concentric grey circles around standard deviation ratio of 1 and correlation of 1) is generally below 0.8. Exceptions are the eastern northern hemisphere polar stations at 250 hPa, the southern hemisphere polar stations at 500 and 800 hPa, and the southern hemisphere mid latitude stations at 800 hPa. At 250 hPa the correlation is better than 0.7 over most regions, and exceptionally good results are obtained over the northern hemisphere western polar region. The correlation slightly worsens at 500 and 800 hPa, but generally remains better than 0.6. Across all 42 sites, the average correlation coefficients at 250, 500, and 800 hPa are 0.59, 0.59, and 0.68, respectively. If we leave out the Tropics, which have the worst correlation, they increase to 0.68, 0.68, and 0.73, respectively.

Hence, as a summary, we can state that tropospheric ozone in the reference run is very well simulated with two exceptions: 1) there is a severe underestimate at high northern latitude sites at 250 hPa, and 2) the (small) seasonal cycle over the tropics is not well captured.

Geosci. Model Dev. Discuss., https://doi.org/10.5194/gmd-2017-191
Manuscript under review for journal Geosci. Model Dev.
Discussion started: 3 November 2017

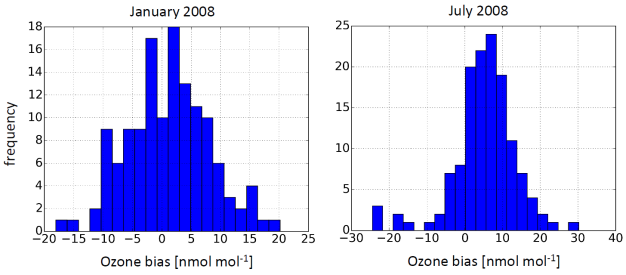

Figure 8. Monthly mean bias of surface ozone mixing ratios in January and July 2008 for all 5 °× 5 °grid boxes where the TOAR database contains data in 2008.

5.3 Surface ozone

For the evaluation of ECHAM-HAMMOZ with surface ozone observations, we make use of the recently published database from the Tropospheric Ozone Assessment Report (TOAR). As described in Schultz et al. (2017), this database contains hourly data from more than 9,000 scientific and air quality monitoring stations worldwide, and it has a globally consistent classification scheme to distinguish urban from rural locations. The classification scheme is based on threshold combinations of global satellite data products of nighttime light intensity, population density, and OMI NO_2 columns. For details see Schultz et al. (2017).

Figure 7 shows gridded maps of TOAR data at rural stations (top row) in comparison with ECHAM-HAMMOZ reference run output regridded to the same resolution of 5 °× 5 °for January and July 2008. The first thing that becomes apparent in Figure 7 is the evident geographical bias of the observations database. About 3/4 of the grid boxes with measurements by rural stations are located either in Europe or North America, and the rest is scattered across the world. The problem of insufficient observational coverage of reactive gases measurements is widely known, and the community yet has to develop a sound strategy how to deal with it.

Where measurements exist, the model generally shows good agreement with the observations in both January and July. During the boreal summer, ozone over the Eastern US and the North Sea/Baltic sea region is somewhat overestimated. Closer inspection reveals differences of up to -25 and +30 ppbv in individual grid boxes. However, altogether the model yields excellent agreement with mean bias of 1.13 $\mathrm{nmol/mol}$ in January, and 5.28 $\mathrm{nmol\,mol^{-1}}$ in July (Figure 8). Additional information, also concerning the sensitivity experiments lght*2 and lght*4 can be found in supplement 3, Figures S3.3 and S3.4. Mean biases increase by 13 % and 31 % for lght*2 and lght*4, respectively.

5.4 Total column CO

Figure 9 shows seasonal mean total column CO from ECHAM-HAMMOZ in comparison to the IASI retrievals. The model reproduces many features of the retrieval very well, but also shows a couple of differences: 1) in fire emissions regions (e.g., over Africa and tropical fires) and in regions with large anthropogenic emissions (e.g., over China) the model CO total columns

Geosci. Model Dev. Discuss., https://doi.org/10.5194/gmd-2017-191
Manuscript under review for journal Geosci. Model Dev.
Discussion started: 3 November 2017

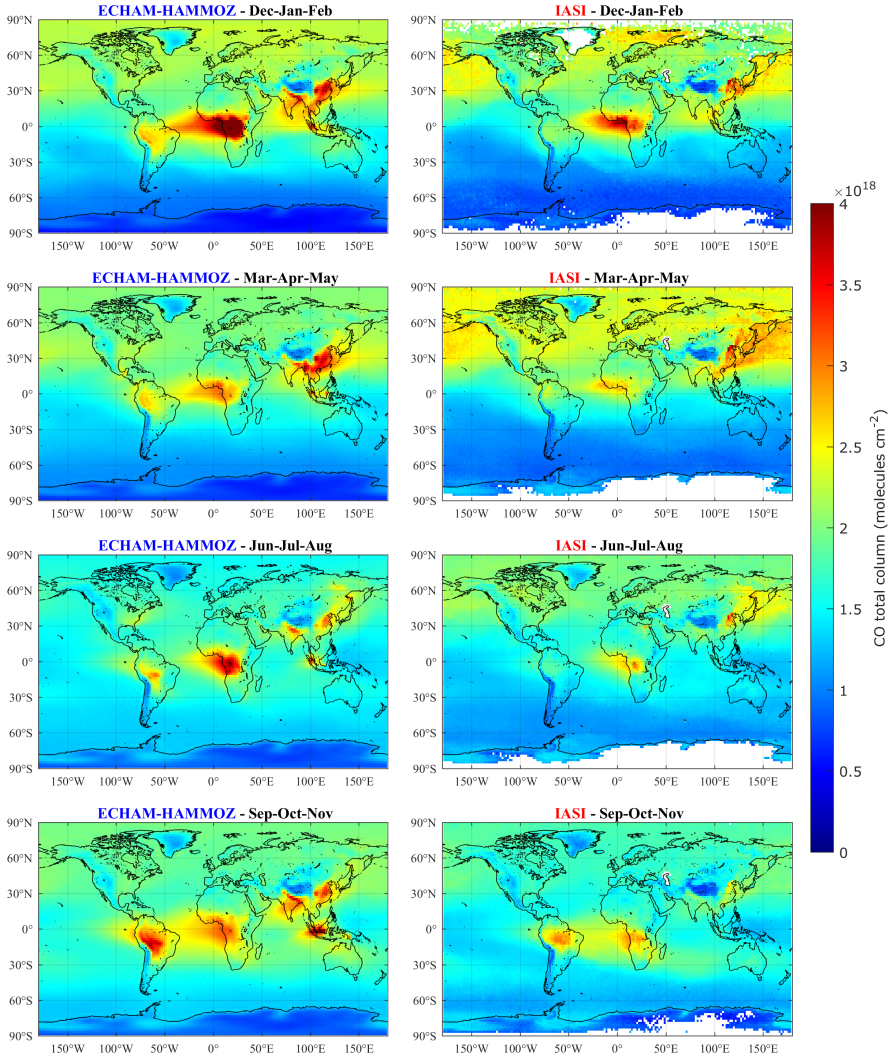

Figure 9. Comparison of seasonal mean total column CO (in 10^{18} cm^{-2}) by ECHAM-HAMMOZ with data from the IASI instrument. Data and model results are from 2008; IASI data were interpolated to the model grid.

appear to be overestimated by a factor of 1.5 with respect to IASI; 2) ECHAM-HAMMOZ appears to lose CO too quickly over the Northern hemisphere in spring and shows a CO seasonality with earlier maximum and minimum (in summer and in winter, respectively) relative to the seasonality derived from IASI. These differences can be explained by the limited sensitivity of IASI in the lowermost layers (George et al., 2015). As a consequence, IASI under-represents the contribution of surface CO to the total column and is more sensitive to CO produced and transported in the mid-troposphere. Moreover, these different vertical sensitivities may affect the representation of the CO seasonality. Indeed, mid-tropospheric CO measurements (including

Geosci. Model Dev. Discuss., https://doi.org/10.5194/gmd-2017-191
Manuscript under review for journal Geosci. Model Dev.
Discussion started: 3 November 2017

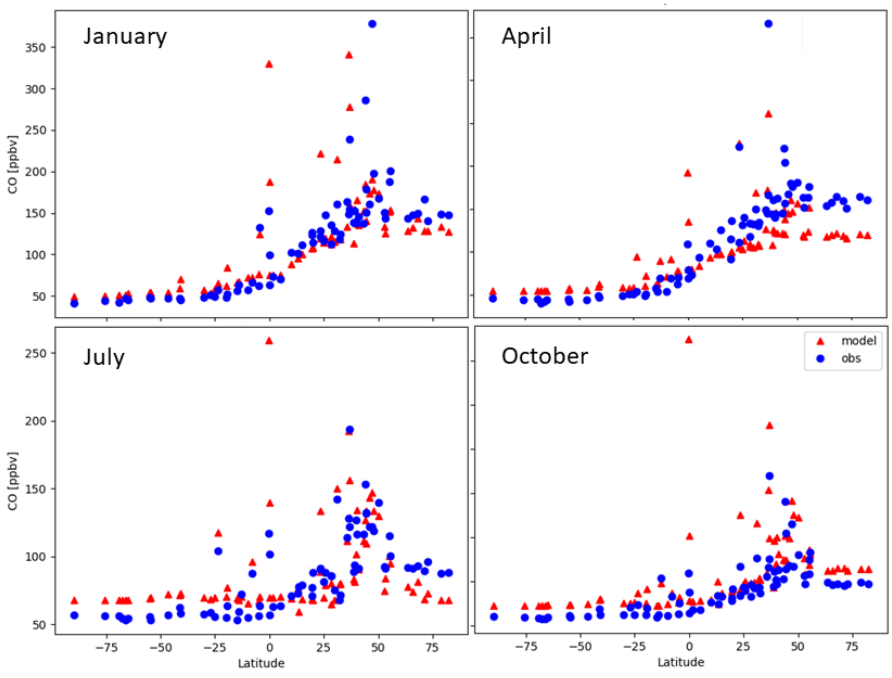

Figure 10. Comparison of monthly mean surface CO measurements from GAW with ECHAM-HAMMOZ reference run results for January, April, July, and October 2008. Each symbol represents data of one measurement location.

IASI observations) have been shown to present a 2-month time lag in the Northern hemisphere CO seasonality compared to measurements from the planetary boundary layer, which are directly influenced by CO emissions (Té et al., 2016).

5.5 Surface CO

Figure 10 displays the latitudional gradients of surface CO concentrations from the World Meteorological Organisation Global Atmosphere Watch (GAW) network (cf. Schultz et al., 2015) in comparison with ECHAM-HAMMOZ reference run results for the year 2008. In general, the model captures the latitudinal variations of CO well throughout the year. However, in higher northern latitudes the simulated CO is underestimated by up to 40 ppbv (33%) in April and to a lesser degree also in January. Reasons for such model-observation discrepancies have been discussed in Stein et al. (2014) and are likely related to inaccurate emissions data in combination with excessive dry deposition of CO. The tendency of ECHAM-HAMMOZ to generate too much OH (see section 6) could also play a role here. The model also overestimates CO in the southern hemisphere. This bias is largest during austral winter (up to 15 ppbv, i.e. 30 %). Reasons for this bias are unclear at present, but could be related to excessive emissions from biomass burning (see section 5.4).

Geosci. Model Dev. Discuss., https://doi.org/10.5194/gmd-2017-191
Manuscript under review for journal Geosci. Model Dev.
Discussion started: 3 November 2017

Geoscientific Model Development Discussions

Table 5. Global tropospheric ozone budgets and tropospheric methane lifetimes of the four ECHAM-HAMMOZ simulations described in Table4. An ozone threshold of 150 $\mathrm{nmol\,mol^{-1}}$ is used to denote the tropopause. For comparison, multi-model mean values from Stevenson et al. (2006) and Young et al. (2013) and Naik et al. (2013) and the "GEOS5" budget terms from Lamarque et al. (2012) are also included.

Name Units	O_3 burden Tg	Production $\mathrm{Tg\,yr^{-1}}$	Loss $\mathrm{Tg\,yr^{-1}}$	Net. Chem. $\mathrm{Tg\,yr^{-1}}$	Deposition $\mathrm{Tg\,yr^{-1}}$	STE $\mathrm{Tg\,yr^{-1}}$	Lifetime days	CH_4 lifetime[a] years	Avg. OH 10^5molec. $\mathrm{cm^{-3}}$
reference	321	5309	4866	443	791	348	24.1	9.87 (8.56)	10.6
lght*2	347	5752	5254	497	821	324	24.1	9.15 (7.90)	11.8
lght*4	382	6357	5794	563	868	305	24.1	8.28 (7.11)	13.5
no_het_HNO_3	337	5620	5083	537	923	386	24.2	9.22 (7.94)	11.4
Stevenson et al. (2006)[b c]	336 ± 27	4974 ± 223	4577 ± 291	397	953 ± 154	556 ± 154	22.2 ± 2.2		
Young et al. (2013)[d]	337 ± 23	5110 ± 606	4668 ± 727	442	1003 ± 200	552 ± 168	22.3 ± 2.0		
Naik et al. (2013)[c]								9.7 ± 1.5	11.1 ± 1.6
Lamarque et al. (2012)[e]	328	4897	4604	293	705	411	26.0	8.7	
Jöckel et al. (2016)								(7.65)	

[a] Computed as whole atmosphere burden of CH_4 over tropospheric loss of CH_4 as in Naik et al. (2013). Values in parantheses were computed according to Jöckel et al. (2016) as tropospheric CH_4 burden over tropospheric CH_4 loss. [b] Values from selected models with relatively low O_3 bias and CH_4 lifetime close to the multi-model mean [c] Year 2000 results. [d] Burden from 15 ACCMIP models, budget terms from 6 models. [e] Tropopause threshold at $O_3 < 100\mathrm{nmol\,mol^{-1}}$.

6 Global budgets

6.1 Ozone and OH

The global budgets of ozone, and the tropospheric methane lifetime of the ECHAM-HAMMOZ reference run are in the range of estimates from other recent models and model intercomparison studies (Table 5). The reference run ozone burden is about 15 Tg lower than the averages of the multi-model studies, but well within the standard deviation. Production and loss terms are above the average plus one standard deviation of the selected models in Stevenson et al. (2006), but well in the range of models reported by Young et al. (2013). Since the HAMMOZ chemical mechanism resembles the CAM-Chem mechanism to a substantial degree, one might expect a better agreement to Lamarque et al. (2012), who report substantially lower values. However, Lamarque et al. (2012) used an ozone threshold of 100 $\mathrm{nmol\,mol^{-1}}$ for the tropopause definition, whereas all other studies in Table 5 used a threshold of 150 $\mathrm{nmol\,mol^{-1}}$. If we evaluate the reference run ozone budget with a 100 $\mathrm{nmol\,mol^{-1}}$ threshold, we obtain a burden of 292 Tg, and production and loss rates of 5192 $\mathrm{Tg\,yr^{-1}}$ and 4807 $\mathrm{Tg\,yr^{-1}}$, respectively.

The above-average ozone production and loss rates are most likely due to the more detailed VOC mechanism in ECHAM-HAMMOZ. Stevenson et al. (2006) already noted that earlier model simulations with fewer primary VOC species tended to yield lower production and loss rates. Considering that our reference run has very low lightning NO_x emissions (at the low end of the models described in Young et al. (2013)), it is indeed astonishing that our ozone chemistry is so active while at the same time the ozone lifetime is about 10% longer than the multi-model averages of Stevenson et al. (2006) and Young et al. (2013). On the other hand it is also 20% shorter than the result reported by Lamarque et al. (2012) (22.2 days if we use the tropopause threshold of $O_3 < 100\mathrm{nmol\,mol^{-1}}$). As noted by Young et al. (2013): "Despite general agreement on how the drivers impact global-scale shifts in tropospheric ozone, magnitudes of the regional changes and the overall ozone budget vary

Geosci. Model Dev. Discuss., https://doi.org/10.5194/gmd-2017-191
Manuscript under review for journal Geosci. Model Dev.
Discussion started: 3 November 2017

Geoscientific Model Development Discussions

Table 6. Percent changes in ozone budget terms in the northern hemisphere, the southern hemisphere, and the tropics of the simulations lght*2 and lght*4 versus the reference run. The latitude boundary of the tropics was chosen at 20° N or S.

Region	O_3 burden	Production	Loss
Run lght*2			
NH	4%	2%	3%
SH	8%	6%	8%
Tropics	14%	14%	11%
Global	8%	8%	8%
Run lght*4			
NH	9%	4%	8%
SH	18%	15%	20%
Tropics	32%	33%	26%
Global	19%	20%	19%

considerably between different models." In ECHAM-HAMMOZ the tropical upper troposphere appears to play a prominent role for the global tropospheric trace gas budgets as evidenced by our lightning NO_x sensitivity simulations. Table 6 lists the percent changes in the ozone budget terms when we double or quadruple the lightning NO_x emissions. The tropics are the region with the highest frequency of thunderstorms and the highest flash density (Boccippio et al., 2000), and we do find the largest changes of the ozone budget in this region. For example, the chemical production of ozone increases by 33% if we increase the lightning NO_x emissions to 4.8 $\mathrm{Tg(N)\,yr^{-1}}$, a value close to the mean or median lightning NO_x emissions of the models described in Young et al. (2013). The global increase in the ozone production is 1047 $\mathrm{Tg\,yr^{-1}}$ (Table 5), and the increase in the tropics constitutes 80% of this change. The northern hemisphere is least affected by the increased lightning NO_x source due to the much larger surface and aircraft emissions in this region. This is also reflected in the evaluation of the model runs with surface ozone observations (see section 5.3): in spite of the large changes in the global budget terms and the substantial increase in the global burden in the lght*4 run, the mean bias in comparison with the gridded TOAR dataset of rural stations increases only moderately from 5.3 $\mathrm{nmol\,mol^{-1}}$ to 6.9 $\mathrm{nmol\,mol^{-1}}$. The density of stations in the northern hemisphere is much greater than elsewhere, so that the larger changes in surface ozone in the tropics and southern hemisphere (see Figure S3.3) are not accounted for in the bias calculation (Figure S3.4).

The tropospheric average OH concentration ($10.6 \cdot 10^5$ $\mathrm{molec.cm^{-3}}$ and methane lifetime (9.87 years) of our reference run are close to the multi-model average diagnosed by Naik et al. (2013) ($11.1 \cdot 10^5$ $\mathrm{molec.cm^{-3}}$ and 9.7 years, respectively). If we increase lightning NO_x emissions, OH increases and the CH_4 lifetime decreases as expected. With 4.8 $\mathrm{Tg(N)\,yr^{-1}}$ as global lightning source, the CH_4 lifetime is 8.28 years, which is more than two standard deviations below the observational constraints from either Prinn et al. (2005) or Prather et al. (2012). However, our CH_4 lifetime appears rather consistent with the lifetime of Jöckel et al. (2016), who use a different method for the calculation (see footnote a of Table 5). Their year-2008 lifetime of

Geosci. Model Dev. Discuss., https://doi.org/10.5194/gmd-2017-191
Manuscript under review for journal Geosci. Model Dev.
Discussion started: 3 November 2017

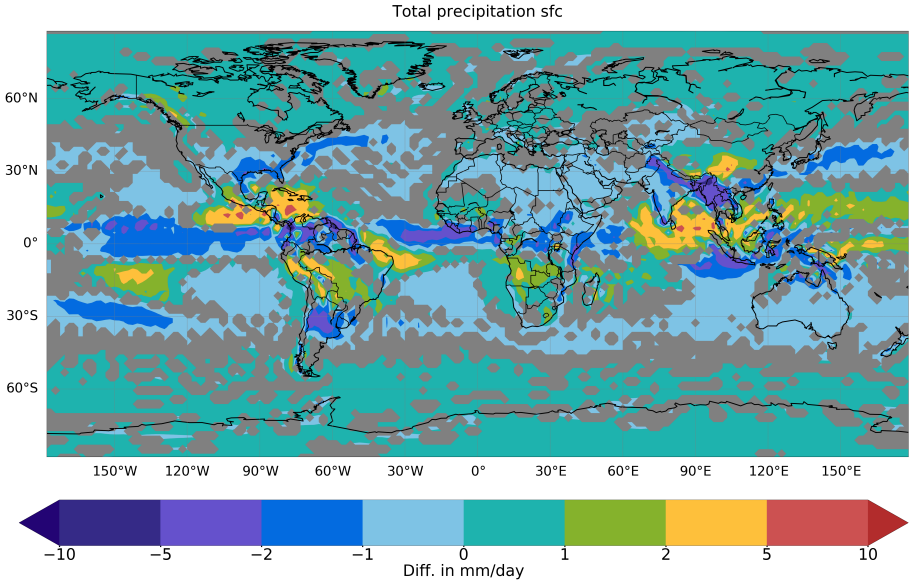

Figure 11. Decadal mean bias of total precipitation in ECHAM6.3 compared to the ECMWF ERA-Interim reanalysis (Dee et al., 2011). Figure re-generated from data described in Krefting (2017).

7.65 years falls between our lght*2 and lght*4 simulations if we apply the same method as Jöckel et al. (2016). Given that their lightning NO_x emissions were about 4 $Tg(N)\,yr^{-1}$ during this period, the agreement is remarkable. As a consequence we note that chemistry models which use the dynamical core and physics of ECHAM have a tendency to be too reactive and generate too much OH. This has already been an issue of earlier ECHAM-HAMMOZ model versions (e.g. Rast et al., 2014). Indeed, Baumgärtner et al. (2016) have shown that the dynamical core can have a large impact on the global CH_4 lifetime. If we put this information in context with the analysis of regional ozone budget changes due to lightning NO_x emission changes, we hypothesize that there is some issue with the dynamics or physics of ECHAM in the tropical troposphere that impacts on its ability to reproduce the global budgets of reactive trace gases. A further hint in this direction is given by Stevens et al. (2013), who pointed out that both ECHAM5 (which forms the basis of the EMAC model reported by Jöckel et al. (2016)) and ECHAM6 (the basis of ECHAM-HAMMOZ as described here) have a tropical precipitation bias of up to 5 $mm\,day^{-1}$. Figure 11 shows the difference in total precipitation between a decadal ECHAM6.3 simulation (i.e. the ECHAM-HAMMOZ model without the chemistry and aerosol schemes) versus the ERA-Interim reanalysis (Dee et al., 2011), which confirms the statement of Stevens et al. (2013). A more detailed investigation of this issue is beyond the scope of this paper.

6.2 NO_x budget

The global NO_x budget of the reference run differs somewhat from other estimates (e.g. Xu and Penner, 2012) as can be seen from Table 7. While the total NO_x emissions (except for lightning as discussed above) are very similar to other recent studies, the dry and wet deposition rates are about a factor of three lower. This is due to the parameterisation of the heterogeneous

Geosci. Model Dev. Discuss., https://doi.org/10.5194/gmd-2017-191
Manuscript under review for journal Geosci. Model Dev.
Discussion started: 3 November 2017

Geoscientific Model Development Discussions

Table 7. Global tropospheric NO_x budgets of the four ECHAM-HAMMOZ simulations described in Table4.

Name Units	NO_x emissions $Tg(N)\,yr^{-1}$	HNO_3 dry deposition $Tg(N)\,yr^{-1}$	HNO_3 wet deposition $Tg(N)\,yr^{-1}$	$HNO_3 \rightarrow NO_2$ $Tg(N)\,yr^{-1}$	HNO_3 burden $Tg(N)$
reference	45.5	3.58	7.01	0.92	0.08
no_het_HNO_3	45.5	11.08	24.48	2.99	0.31
Xu and Penner (2012)[a]	41.0	11.75	26.44	4.31	0.30
Feng and Penner (2007)[a]	38.9	10.5	25.5	N.A.	0.37
Rodriguez and Dabdub (2004)[a]	34.7	5.1	24.6	N.A.	N.A.
Liao et al. (2004)[a]	40.0	14.0	14.3	N.A.	0.28

[a] These studies distinguish between gas-phase and nitrate aerosol, while ECHAM-HAMMOZ does not have nitrate aerosol as a separate tracer. The deposition rates listed in this table are total nitrate deposition.

uptake of HNO_3 on seasalt and dust aerosols, which removes HNO_3 from the system and does not allow for re-evaporation from the aerosol or droplet phase. The sensitivity run no_het_HNO3 yields dry and wet deposition rates of nitrogen which are very close to Xu and Penner (2012) and in the range of other model studies (Liao et al., 2004; Rodriguez and Dabdub, 2004; Feng and Penner, 2007).

6.3 Radiation, clouds and aerosol

Even though the focus of this paper is the tropospheric and stratospheric gas-phase chemistry in ECHAM-HAMMOZ, it is useful to evaluate aerosol burdens, and cloud and radiation fields in order to assess how the comprehensive gas-phase chemistry mechanism of MOZ relates to HAM-only simulations and other studies. This section focuses on 10-year global mean values of radiation, cloud and aerosol variables. Spatial distribution maps of speciated aerosol mass burdens and time series of seasonal aerosol burden means are contained in the supplementary material. A more extensive evaluation of the radiation, clouds and aerosols in ECHAM6.3-HAM2.3 will be provided in the forthcoming papers of Tegen et al. (in preparation), Kokkola et al. (in preparation), Kühn, et al. (in preparation), and Neubauer et al. (in preparation).

Global 10-year mean values of the top of the atmosphere (TOA) energy budget, cloud related properties and aerosol mass burdens are shown in Table 8 for the ECHAM- HAMMOZ base simulation, reference simulations of ECHAM6.1-HAM2.2 and ECHAM6.3-HAM2.3 and observations as well as AeroCom multi model mean values. The spatial distribution global maps of aerosol burden can be found in Figure S3.5 of the supplementary material. The settings of ECHAM6.3-HAM2.3 and ECHAM6.1-HAM2.2 simulations are similar to the ECHAM-HAMMOZ base simulation except that MOZ1.0 is not used, the modal aerosol module M7 is used and the temperature is not nudged. The ECHAM6.3-HAM2.3 simulation uses a different sea salt aerosol particles emission parameterization (Long et al., 2011). Therefore the ECHAM6.1-HAM2.2 simulation is also included in Table 8 as it uses the same parameterization of Guelle et al. (2001) for sea salt emissions as the ECHAM-HAMMOZ base simulation. The reference time range for ECHAM6.1-HAM2.2 was 2000-2009, so we keep this time range to be consistent

Geosci. Model Dev. Discuss., https://doi.org/10.5194/gmd-2017-191
Manuscript under review for journal Geosci. Model Dev.
Discussion started: 3 November 2017

Geoscientific Model Development Discussions
Open Access
EGU

Table 8. Global annual mean top of the atmosphere (TOA) energy budget, cloud related properties and aerosol mass burdens of the base simulation, the ECHAM6.3-HAM2.3 (E63H23) and ECHAM6.1-HAM2.2 (E61H22) climate simulations and observations or multi-model mean values. All ECHAM simulations are decadal averages (2003-2012).

	reference	E63H23	E61H22	Observed/Multi model mean
Shortwave net at TOA ($\mathrm{W\,m^{-2}}$)	245.1	239.5	237.4	240.0[a]
Shortwave cloud radiative effect TOA ($\mathrm{W\,m^{-2}}$)	-42.5	-48.4	-49.5	-47.3[b]
Longwave net at TOA ($\mathrm{W\,m^{-2}}$)	-240.5	-240.0	-238.3	239.0[a]
Longwave cloud radiative effect TOA ($\mathrm{W\,m^{-2}}$)	21.4	23.2	25.1	26.2[b]
Net cloud radiative effect TOA ($\mathrm{W\,m^{-2}}$)	-21.1	-25.3	-24.4	-21.1[b]
Imbalance TOA ($\mathrm{W\,m^{-2}}$)	4.6	-0.5	-1.3	0.7[c]
Total cloud cover (%)	63.5	66.2	61.1	68.0[d]
Liquid water path (only for oceans) ($\mathrm{g\,m^{-2}}$)	56.0	69.1	93.0	81.4[e]
Ice water path ($\mathrm{g\,m^{-2}}$)	13.8	14.6	10.3	25.0[f]
Water vapor path ($\mathrm{kg\,m^{-2}}$)	25.4	26.0	25.0	25.2[g]
Total precipitation ($\mathrm{mm\,d^{-1}}$)	3.0	3.0	3.0	2.7[b]
Sulfate burden (Tg)	1.83	2.33	1.92	1.99 ($\pm$25%)[h]
Black carbon burden (Tg)	0.15	0.14	0.15	0.24 ($\pm$42%)[h]
Particulate organic matter burden (Tg)	0.80	1.05	1.17	1.70 ($\pm$27%)[h]
Sea salt burden (Tg)	9.3	3.9	10.7	7.5 ($\pm$54%)[h]
Mineral dust burden (Tg)	20.9	18.8	13.7	19.2 ($\pm$40%)[h]

[a] Taken from Fig. 1 of Wild et al. (2013). [b] Taken from Fig. 7.7 in Boucher et al. (2013); see references therein. [c] Johnson et al. (2016). [d] Stubenrauch et al. (2013). [e] Elsaesser et al. (2017). [f] Taken from Fig. 2 of Li et al. (2012). [g] Average of Table S1 of von der Haar et al. (2012). [h] Taken from Table 10 of Textor et al. (2006).

with the literature, while the HAMMOZ consortium decided that the reference for ECHAM6.3- HAM2.3-MOZ1.0 is 2003-2012 (see Section 4).

The shortwave (SW), resp. longwave (LW) cloud radiative effects (CRE) are weaker in the ECHAM-HAMMOZ simulation by about 6, resp. 2 $\mathrm{W/m^2}$ (SWCRE, resp. LWCRE) than in ECHAM6.3-HAM2.3 and by about 5, resp. 5 $\mathrm{W/m^2}$ (SWCRE, resp. LWCRE) than in the observations. This leads to larger net shortwave fluxes TOA and an imbalance of the radiative fluxes TOA of 4.6 $\mathrm{W/m^2}$. The weaker cloud radiative effects can be explained by a lower cloud cover and a smaller liquid water path in the ECHAM-HAMMOZ simulation. Analog differences were found by Zhang et al. (2014) for ECHAM6.1-HAM2.2 due to differences in nudging techniques. Zhang et al. (2014) investigated the behavior of aerosol-climate models when different nudging techniques are applied compared to free running simulations. In particular the additional nudging of temperature decreased the cloud radiative effects by about 5, resp. 1 $\mathrm{W/m^2}$ (SWCRE, resp. LWCRE) and liquid water path by about 10 $\mathrm{g/m^2}$ in ECHAM6.1-HAM2.2 compared to only nudging vorticity, divergence and surface pressure. Further changes were a smaller water vapor path and changes in convection when simulations are nudged.

Geosci. Model Dev. Discuss., https://doi.org/10.5194/gmd-2017-191
Manuscript under review for journal Geosci. Model Dev.
Discussion started: 3 November 2017

The 10-year global means of the aerosol mass burdens of the ECHAM-HAMMOZ simulations are comparable with the ECHAM-HAM simulations and AeroCom multi-model mean values Textor et al. (2006). The particulate organic matter burden in ECHAM-HAM(MOZ) simulations is lower than in the AeroCom multi-model mean, which is presumably due to the simplistic treatment of secondary organic aerosols (Zhang et al., 2012). The sea salt burden is larger in the ECHAM-HAMMOZ base simulation than in the corresponding ECHAM6.3-HAM2.3 simulation but this can be explained by the different sea salt emission parameterization as mentioned above. ECHAM6.1-HAM2.2, which uses the same sea salt emission parameterization as the ECHAM- HAMMOZ base simulation (Guelle et al., 2001), has a similar sea salt burden as ECHAM-HAMMOZ.

Overall, the 10-year mean aerosol burden maps (Figure S3.5) show a reasonable comparison between the patterns of ECHAM-HAMMOZ and ECHAM6.3HAM2.3. The sulfate burden (first row of Figure S3.5) is everywhere lower in ECHAM-HAMMOZ than in ECHAM6.3-HAM2.3, but is quite similar to ECHAM6.1-HAM2.2. MOZ1.0 is a gas-phase module which does not interact directly with black carbon, particulate organic matter, sea salt and mineral dust. The aerosol sulfate amount is directly affected by the gas-phase module through the computation of H_2SO_4, therefore some differences between ECHAM-HAMMOZ and ECHAM6-HAM2.3 are expected. However these differences are in the range of the AeroCom models. The spatial distribution of black carbon, particulate organic matter and mineral dust burdens are quite similar in ECHAM-HAMMOZ compared to ECHAM6.3-HAM2.3. For the sea salt burden, the spatial distribution of ECHAM-HAMMOZ agrees quite well with the one of ECHAM6.1-HAM2.2. The seasonal cycles of the global means of aerosol mass burdens in ECHAM-HAMMOZ are very similar to the ones in ECHAM6.3-HAM2.3 and ECHAM6.1-HAM2.2 (Figure S3.6 in supplementary material). The differences are consistent with those dicussed above.

Overall, it can be concluded that the nudged ECHAM-HAMMOZ base simulation produces reasonable results for TOA radiative fluxes, cloud related properties and aerosol mass burdens. All parameters are in the range of other nudged ECHAM-HAM simulations, Aerocom multi-model mean values, and observations. Differences between ECHAM-HAMMOZ and ECHAM6.3-HAM2.3 can be explained by the use of a different aerosol microphysics scheme (Kokkola et al., in preparation; Kühn et al., in preparation), the use of a different sea-salt emissions scheme (see also Tegen et al., in preparation), and different settings for the dynamical nudging (Zhang et al., 2014, ; see also Neubauer et al., in preparation).

7 Conclusions

ECHAM-HAMMOZ in its released version ECHAM6.3-HAM2.3-MOZ1.0 is a state-of-the-art chemistry climate model with a comprehensive tropospheric and stratospheric chemistry package and two options to model aerosol processes with either a modal or a bin scheme.

A ten-year simulation from 2003 to 2012 in the default configuration was performed and has been evaluated with various observational data and compared to other model studies. The focus of the evaluation was placed on the year 2008. The model reproduces many of the observed features of total column ozone, polar stratospheric processes, tropospheric and surface ozone, column and surface CO. Like many other models, ECHAM-HAMMOZ shows a high bias of surface ozone concentrations, but this bias is relatively modest. Global budgets of ozone and OH are in line with estimates from multi-model intercomparison

studies and two individual models using either a similar chemistry scheme (CAM-CHEM), or a similar climate model (EMAC) as ECHAM-HAMMOZ.

The evaluation of the model run in the default configuration revealed two issues with respect to the global NO_x budget: 1) lightning emissions are only about 1.2 $Tg(N)\,yr^{-1}$, and thus a factor two lower than the lower limit that is generally accepted by the community; 2) the parameterisations of heterogeneous reactions constitute a too strong sink of HNO_3. The aerosol model of ECHAM-HAMMOZ does not include explicit treatment of nitrate, and therefore, re-evaporation of HNO_3 that is lost to the aerosol phase is not occurring. Three sensitivity simulations were performed, which corrected these issues. Unfortunately, the results from these simulations tend to increase model biases, and in particular they invigorate the tropospheric ozone chemistry and decrease the lifetime of CH_4. These changes occur almost exclusively in the tropics and may be related to issues with tropical dynamics in the ECHAM model, which also show up as precipitation bias. The evaluation of cloud and radiation budgets hint towards a possible radiative imbalance induced by the nudging set-up. However, the precipitation bias has been found also in other simulations with ECHAM6, and the excessive ozone chemistry and OH concentrations are also a feature of EMAC, which is based on an earlier version of ECHAM (with modifications).

Code and data availability. The ECHAM-HAMMOZ model source code and all required input data are freely available after signature of a license agreement. Further information and the license agreement can be obtained from https://redmine.hammoz.ethz.ch/projects/hammoz/wiki/Echam630-ham23-moz10.

Author contributions. MGS participated in the general code design of ECHAM-HAMMOZ and led the development of the gas-phase chemistry module; he designed this manuscript, performed 40% of the analyses and wrote 65% of the manuscript. ScS contributed to the model development, performed most model simulations, and contributed to the analysis. SaS and SF were pivotal in the technical model development and maintenance of all prior code versions. CSLD managed the model input data and contributed to the model development. All other authors contributed either to the model development or to the model evaluation and contributed individual sections to the manuscript.

Competing interests. The authors declare that they have no competing interests

Acknowledgements. The ECHAM-HAMMOZ model is developed by a consortium composed of ETH Zurich, Max Planck Institut für Meteorologie, Forschungszentrum Jülich, University of Oxford, the Finnish Meteorological Institute and the Leibniz Institute for Tropospheric Research, and managed by the Center for Climate Systems Modeling (C2SM) at ETH Zurich. We wish to thank the C2SM at ETH Zürich for hosting the model code and technical support to model development. JSC is acknowledged for computing time on JURECA (2016) and technical support for implementation of the model on this platform. Specifically, we would like to thank Olaf Stein for his continuous support. The Max-Planck-Institute for Meteorology, Hamburg, Germany, is gratefully acknowledged for developing the ECHAM general circulation

model and making it available to the HAMMOZ community. Charles Bardeen (NCAR) helped to make MLS data available for the evaluation of stratospheric processes. All authors from Forschungszentrum Jülich have been funded through the Helmholtz POF programme. P.S. would like to acknowledge funding by the European Research Council under the European Union's Seventh Framework Programme (FP7/2007–2013)/ERC grant agreement no. FP7– 280025 (ACCLAIM).

References

Aghedo, A. M., Schultz, M. G., and Rast, S.: The influence of African air pollution on regional and global tropospheric ozone, Atmospheric Chemistry and Physics, 7, 1193–1212, 2007.

Auvray, M., Bey, I., Llull, E., Schultz, M. G., and Rast, S.: A model investigation of tropospheric ozone chemical tendencies in long-range transported pollution plumes, Journal of Geophysical Research: Atmospheres, 112, n/a–n/a, https://doi.org/10.1029/2006JD007137, http://dx.doi.org/10.1029/2006JD007137, d05304, 2007.

Baumgärtner, A. J. G., Jöckel, P., Kerkweg, A., Sander, R., and Tost, H.: Implementation of the Community Earth System Model (CESM) version 1.2.1 as a new base model into version 2.50 of the MESSy framework, Geoscientific Model Development, 9, 125–135, https://doi.org/10.5194/gmd-9-125-2016, 2016.

Bergman, T., Kerminen, V. M., Korhonen, H., Lehtinen, K. J., Makkonen, R., Arola, A., Mielonen, T., Romakkaniemi, S., Kulmala, M., and Kokkola, H.: Evaluation of the sectional aerosol microphysics module SALSA implementation in ECHAM5-HAM aerosol-climate model, Geoscientific Model Development, 5, 845–868, https://doi.org/10.5194/gmd-5-845-2012, 2012.

Boccippio, D. J., Goodman, S. J., and Heckman, S.: Regional Differences in Tropical Lightning Distributions, Journal of Applied Meteorology, 39, 2231–2248, https://doi.org/10.1175/1520-0450(2001)040<2231:RDITLD>2.0.CO;2, 2000.

Boucher, O., Randall, D., Artaxo, P., Bretherton, C., Feingold, G., Forster, P., Kerminen, V.-M., Kondo, Y., Liao, H., Lohmann, U., Rasch, P., Satheesh, S., Sherwood, S., Stevens, B., and Zhang, X.: Clouds and aerosols, pp. 571–657, Cambridge University Press, 2013.

Boynard, A., Hurtmans, D., Koukouli, M. E., Goutail, F., Bureau, J., Safieddine, S., Lerot, C., Hadji-Lazaro, J., Wespes, C., Pommereau, J.-P., Pazmino, A., Zyrichidou, I., Balis, D., Barbe, A., Mikhailenko, S. N., Loyola, D., Valks, P., Van Roozendael, M., Coheur, P.-F., and Clerbaux, C.: Seven years of IASI ozone retrievals from FORLI: validation with independent total column and vertical profile measurements, Atmospheric Measurement Techniques, 9, 4327–4353, https://doi.org/10.5194/amt-9-4327-2016, 2016.

Brasseur, G. P., Hauglustaine, D. A., Walters, S., Rasch, P. J., Muller, J. F., Granier, C., and Tie, X. X.: MOZART, a global chemical transport model for ozone and related chemical tracers 1. Model description, Journal of Geophysical Research-Atmospheres, 103, 28 265–28 289, https://doi.org/10.1029/98jd02397, 1998.

Brinkop, S. and Roeckner, E.: SENSITIVITY OF A GENERAL-CIRCULATION MODEL TO PARAMETERIZATIONS OF CLOUD-TURBULENCE INTERACTIONS IN THE ATMOSPHERIC BOUNDARY-LAYER, Tellus Series a-Dynamic Meteorology and Oceanography, 47, 197–220, https://doi.org/10.1034/j.1600-0870.1995.t01-1-00004.x, 1995.

Brovkin, V., Boysen, L., Raddatz, T., Gayler, V., Loew, A., and Claussen, M.: Evaluation of vegetation cover and land-surface albedo in MPI-ESM CMIP5 simulations, Journal of Advances in Modeling Earth Systems, 5, 48–57, https://doi.org/10.1029/2012ms000169, 2013.

Christian, H. J., Blakeslee, R. J., Boccippio, D. J., Boeck, W. L., Buechler, D. E., Driscoll, K. T., Goodman, S. J., Hall, J. M., Koshak, W. J., Mach, D. M., and Stewart, M. F.: Global frequency and distribution of lightning as observed from space by the Optical Transient Detector, Journal of Geophysical Research-Atmospheres, 108, https://doi.org/10.1029/2002jd002347, 2003.

Clerbaux, C., Boynard, A., Clarisse, L., George, M., Hadji-Lazaro, J., Herbin, H., Hurtmans, D., Pommier, M., Razavi, A., Turquety, S., Wespes, C., and Coheur, P.-F.: Monitoring of atmospheric composition using the thermal infrared IASI/MetOp sounder, Atmospheric Chemistry and Physics, 9, 6041–6054, https://doi.org/10.5194/acp-9-6041-2009, 2009.

Croft, B., Lohmann, U., Martin, R. V., Stier, P., Wurzler, S., Feichter, J., Posselt, R., and Ferrachat, S.: Aerosol size-dependent below-cloud scavenging by rain and snow in the ECHAM5-HAM, Atmospheric Chemistry and Physics, 9, 4653–4675, 2009.

Croft, B., Lohmann, U., Martin, R. V., Stier, P., Wurzler, S., Feichter, J., Hoose, C., Heikkila, U., van Donkelaar, A., and Ferrachat, S.: Influences of in-cloud aerosol scavenging parameterizations on aerosol concentrations and wet deposition in ECHAM5-HAM, Atmospheric Chemistry and Physics, 10, 1511–1543, 2010.

Dee, D. P., Uppala, S. M., Simmons, A. J., Berrisford, P., Poli, P., Kobayashi, S., Andrae, U., Balmaseda, M. A., Balsamo, G., Bauer, P., Bechtold, P., Beljaars, A. C. M., van de Berg, L., Bidlot, J., Bormann, N., Delsol, C., Dragani, R., Fuentes, M., Geer, A. J., Haimberger, L., Healy, S. B., Hersbach, H., Holm, E. V., Isaksen, L., Kallberg, P., Kohler, M., Matricardi, M., McNally, A. P., Monge-Sanz, B. M., Morcrette, J. J., Park, B. K., Peubey, C., de Rosnay, P., Tavolato, C., Thepaut, J. N., and Vitart, F.: The ERA-Interim reanalysis: configuration and performance of the data assimilation system, Quarterly Journal of the Royal Meteorological Society, 137, 553–597, https://doi.org/10.1002/qj.828, 2011.

Dentener, F., Kinne, S., Bond, T., Boucher, O., Cofala, J., Generoso, S., Ginoux, P., Gong, S., Hoelzemann, J. J., Ito, A., Marelli, L., Penner, J. E., Putaud, J. P., Textor, C., Schulz, M., van der Werf, G. R., and Wilson, J.: Emissions of primary aerosol and precursor gases in the years 2000 and 1750 prescribed data-sets for AeroCom, Atmospheric Chemistry and Physics, 6, 4321–4344, 2006a.

Dentener, F., Stevenson, D., Ellingsen, K., van Noije, T., Schultz, M., Amann, M., Atherton, C., Bell, N., Bergmann, D., Bey, I., Bouwman, L., Butler, T., Cofala, J., Collins, B., Drevet, J., Doherty, R., Eickhout, B., Eskes, H., Fiore, A., Gauss, M., Hauglustaine, D., Horowitz, L., Isaksen, I. S. A., Josse, B., Lawrence, M., Krol, M., Lamarque, J. F., Montanaro, V., Muller, J. F., Peuch, V. H., Pitari, G., Pyle, J., Rast, S., Rodriguez, J., Sanderson, M., Savage, N. H., Shindell, D., Strahan, S., Szopa, S., Sudo, K., Van Dingenen, R., Wild, O., and Zeng, G.: The global atmospheric environment for the next generation, Environmental Science & Technology, 40, 3586–3594, https://doi.org/10.1021/es0523845, 2006b.

Elsaesser, G., O'Dell, C., Lebsock, M., Bennartz, R., and Greenwald, T.: The Multi-Sensor Advanced Climatology of Liquid Water Path (MAC-LWP), J. Clim., https://doi.org/10.1175/JCLI-D-16-0902.1, 2017.

Emmons, L. K., Apel, E. C., Lamarque, J. F., Hess, P. G., Avery, M., Blake, D., Brune, W., Campos, T., Crawford, J., DeCarlo, P. F., Hall, S., Heikes, B., Holloway, J., Jimenez, J. L., Knapp, D. J., Kok, G., Mena-Carrasco, M., Olson, J., O'Sullivan, D., Sachse, G., Walega, J., Weibring, P., Weinheimer, A., and Wiedinmyer, C.: Impact of Mexico City emissions on regional air quality from MOZART-4 simulations, Atmospheric Chemistry and Physics, 10, 6195–6212, https://doi.org/10.5194/acp-10-6195-2010, 2010.

Eskes, H., Huijnen, V., Arola, A., Benedictow, A., Blechschmidt, A.-M., Botek, E., Boucher, O., Bouarar, I., Chabrillat, S., Cuevas, E., Engelen, R., Flentje, H., Gaudel, A., Griesfeller, J., Jones, L., Kapsomenakis, J., Katragkou, E., Kinne, S., Langerock, B., Razinger, M., Richter, A., Schultz, M., Schulz, M., Sudarchikova, N., Thouret, V., Vrekoussis, M., Wagner, A., and Zerefos, C.: Validation of reactive gases and aerosols in the MACC global analysis and forecast system, Geoscientific Model Development, 8, 3523–3543, https://doi.org/10.5194/gmd-8-3523-2015, 2015.

Eyring, V., Arblaster, J. M., Cionni, I., Sedlacek, J., Perliwitz, J., Young, P. J., Bekki, S., Bergmann, D., Cameron-Smith, P., Collins, W. J., Faluvegi, G., Gottschaldt, K. D., Horowitz, L. W., Kinnison, D. E., Lamarque, J. F., Marsh, D. R., Saint-Martin, D., Shindell, D. T., Sudo, K., Szopa, S., and Watanabe, S.: Long-term ozone changes and associated climate impacts in CMIP5 simulations, Journal of Geophysical Research-Atmospheres, 118, 5029–5060, https://doi.org/10.1002/jgrd.50316, 2013.

Fadnavis, S., Semeniuk, K., Pozzoli, L., Schultz, M. G., Ghude, S. D., Das, S., and Kakatkar, R.: Transport of aerosols into the UTLS and their impact on the Asian monsoon region as seen in a global model simulation, Atmospheric Chemistry and Physics, 13, 8771–8786, https://doi.org/10.5194/acp-13-8771-2013, 2013.

Fadnavis, S., Schultz, M. G., Semeniuk, K., Mahajan, A. S., Pozzoli, L., Sonbawne, S., Ghude, S. D., Kiefer, M., and Eckert, E.: Trends in peroxyacetyl nitrate (PAN) in the upper troposphere and lower stratosphere over southern Asia during the summer monsoon season: regional impacts, Atmospheric Chemistry and Physics, 14, 12 725–12 743, https://doi.org/10.5194/acp-14-12725-2014, 2014.

Fadnavis, S., Semeniuk, K., Schultz, M. G., Kiefer, M., Mahajan, A., Pozzoli, L., and Sonbawane, S.: Transport pathways of peroxyacetyl nitrate in the upper troposphere and lower stratosphere from different monsoon systems during the summer monsoon season, Atmospheric Chemistry and Physics, 15, 11 477–11 499, https://doi.org/10.5194/acp-15-11477-2015, 2015.

Feng, Y. and Penner, J. E.: Global modeling of nitrate and ammonium: Interaction of aerosols and tropospheric chemistry, J. Geophys. Res., 112, https://doi.org/10.1029/2005JD006404, 2007.

Ganzeveld, L. and Lelieveld, J.: DRY DEPOSITION PARAMETERIZATION IN A CHEMISTRY GENERAL-CIRCULATION MODEL AND ITS INFLUENCE ON THE DISTRIBUTION OF REACTIVE TRACE GASES, Journal of Geophysical Research-Atmospheres, 100, 20 999–21 012, https://doi.org/10.1029/95jd02266, 1995.

George, M., Clerbaux, C., Bouarar, I., Coheur, P.-F., Deeter, M. N., Edwards, D. P., Francis, G., Gille, J. C., Hadji-Lazaro, J., Hurtmans, D., Inness, A., Mao, D., and Worden, H. M.: An examination of the long-term CO records from MOPITT and IASI: comparison of retrieval methodology, Atmospheric Measurement Techniques, 8, 4313–4328, https://doi.org/10.5194/amt-8-4313-2015, 2015.

Ghan, S., Wang, M. H., Zhang, S. P., Ferrachat, S., Gettelman, A., Griesfeller, J., Kipling, Z., Lohmann, U., Morrison, H., Neubauer, D., Partridge, D. G., Stier, P., Takemura, T., Wang, H. L., and Zhang, K.: Challenges in constraining anthropogenic aerosol effects on cloud radiative forcing using present-day spatiotemporal variability, Proceedings of the National Academy of Sciences of the United States of America, 113, 5804–5811, https://doi.org/10.1073/pnas.1514036113, 2016.

Giorgetta, M., Jungclaus, J., Reick, C., Legutke, S., Brovkin, V., Crueger, T., Esch, M., Fieg, K., Glushak, K., Gayler, V., Haak, H., Hollweg, H.-D., Kinne, S., Kornblueh, L., Matei, D., Mauritsen, T., Mikolajewicz, U., Müller, W., Notz, D., Raddatz, T., Rast, S., Roeckner, E., Salzmann, M., Schmidt, H., Schnur, R., Segschneider, J., Six, K., Stockhause, M., Wegner, J., Widmann, H., Wieners, K.-H., Claussen, M., Marotzke, J., and Stevens, B.: CMIP5 simulations of the Max Planck Institute for Meteorology (MPI-M) based on the MPI-ESM-LR model: The amip experiment, served by ESGF, World Data Center for Climate (WDCC) at DKRZ, https://doi.org/https://doi.org/10.1594/WDCC/CMIP5.MXELam, 2012.

Granier, C., Guenther, A., Lamarque, J., Mieville, A., Muller, J., Olivier, J., Orlando, J., Peters, J., Petron, G., Tyndall, G., and Wallens, S.: POET, a database of surface emissions of ozone precursors, available on the internet at: http://www.aero.jussieu.fr/projet/ACCENT/POET.php, http://www.aero.jussieu.fr/projet/ACCENT/POET.php, 2005.

Granier, C., Bessagnet, B., Bond, T., D'Angiola, A., van der Gon, H. D., Frost, G. J., Heil, A., Kaiser, J. W., Kinne, S., Klimont, Z., Kloster, S., Lamarque, J. F., Liousse, C., Masui, T., Meleux, F., Mieville, A., Ohara, T., Raut, J. C., Riahi, K., Schultz, M. G., Smith, S. J., Thompson, A., van Aardenne, J., van der Werf, G. R., and van Vuuren, D. P.: Evolution of anthropogenic and biomass burning emissions of air pollutants at global and regional scales during the 1980-2010 period, Climatic Change, 109, 163–190, https://doi.org/10.1007/s10584-011-0154-1, 2011.

Grewe, V., Brunner, D., Dameris, M., Grenfell, J. L., Hein, R., Shindell, D., and Staehelin, J.: Origin and variability of upper tropospheric nitrogen oxides and ozone at northern mid-latitudes, Atmospheric Environment, 35, 3421–3433, https://doi.org/10.1016/s1352-2310(01)00134-0, 2001.

Guelle, W., Schulz, M., Balkanski, Y., and Dentener, F.: Influence of the source formulation on modeling the atmospheric global distribution of sea salt aerosol, Journal of Geophysical Research-Atmospheres, 106, 27 509–27 524, https://doi.org/10.1029/2001jd900249, 2001.

Guenther, A. B., Jiang, X., Heald, C. L., Sakulyanontvittaya, T., Duhl, T., Emmons, L. K., and Wang, X.: The Model of Emissions of Gases and Aerosols from Nature version 2.1 (MEGAN2.1): an extended and updated framework for modeling biogenic emissions, Geoscientific Model Development, 5, 1471–1492, https://doi.org/10.5194/gmd-5-1471-2012, 2012.

Gutman, G., Tarpley, D., Ignatov, A., and Olson, S.: THE ENHANCED NOAA GLOBAL LAND DATASET FROM THE ADVANCED VERY HIGH-RESOLUTION RADIOMETER, Bulletin of the American Meteorological Society, 76, 1141–1156, https://doi.org/10.1175/1520-0477(1995)076<1141:tengld>2.0.co;2, 1995.

Hagemann, S. and Stacke, T.: Impact of the soil hydrology scheme on simulated soil moisture memory, Climate Dynamics, 44, 1731–1750, https://doi.org/10.1007/s00382-014-2221-6, 2015.

Harrison, J. J., Chipperfield, M. P., Boone, C. D., Dhomse, S. S., Bernath, P. F., Froidevaux, L., Anderson, J., and Russell, J.: Satellite observations of stratospheric hydrogen fluoride and comparisons with SLIMCAT calculations, Atmospheric Chemistry and Physics, 16, 10 501–10 519, https://doi.org/10.5194/acp-16-10501-2016, 2016.

Henrot, A. J., Stanelle, T., Schroder, S., Siegenthaler, C., Taraborrelli, D., and Schultz, M. G.: Implementation of the MEGAN (v2.1) biogenic emission model in the ECHAM6-HAMMOZ chemistry climate model, Geoscientific Model Development, 10, 903–926, https://doi.org/10.5194/gmd-10-903-2017, 2017.

Hilton, F., Armante, R., August, T., Barnet, C., Bouchard, A., Camy-Peyret, C., Capelle, V., Clarisse, L., Clerbaux, C., Coheur, P.-F., Collard, A., Crevoisier, C., Dufour, G., Edwards, D., Faijan, F., Fourrié, N., Gambacorta, A., Goldberg, M., Guidard, V., Hurtmans, D., Illingworth, S., Jacquinet-Husson, N., Kerzenmacher, T., Klaes, D., Lavanant, L., Masiello, G., Matricardi, M., McNally, A., Newman, S., Pavelin, E., Payan, S., Péquignot, E., Peyridieu, S., Phulpin, T., Remedios, J., Schlüssel, P., Serio, C., Strow, L., Stubenrauch, C., Taylor, J., Tobin, D., Wolf, W., and Zhou, D.: Hyperspectral Earth Observation from IASI: Five Years of Accomplishments, Bulletin of the American Meteorological Society, 93, 347–370, https://doi.org/10.1175/BAMS-D-11-00027.1, 2012.

Hines, C. O.: Doppler-spread parameterization of gravity-wave momentum deposition in the middle atmosphere. Part 1: Basic formulation, Journal of Atmospheric and Solar-Terrestrial Physics, 59, 371 – 386, https://doi.org/http://dx.doi.org/10.1016/S1364-6826(96)00079-X, 1997a.

Hines, C. O.: Doppler-spread parameterization of gravity-wave momentum deposition in the middle atmosphere. Part 2: Broad and quasi monochromatic spectra, and implementation, Journal of Atmospheric and Solar-Terrestrial Physics, 59, 387 – 400, https://doi.org/10.1016/s1364-6826(96)00080-6, 1997b.

Hurtmans, D., Coheur, P.-F., Wespes, C., Clarisse, L., Scharf, O., Clerbaux, C., Hadji-Lazaro, J., George, M., and Turquety, S.: FORLI radiative transfer and retrieval code for IASI, Journal of Quantitative Spectroscopy and Radiative Transfer, 113, 1391 – 1408, https://doi.org/http://dx.doi.org/10.1016/j.jqsrt.2012.02.036, three Leaders in Spectroscopy, 2012.

Iacono, M. J., Delamere, J. S., Mlawer, E. J., Shephard, M. W., Clough, S. A., and Collins, W. D.: Radiative forcing by long-lived greenhouse gases: Calculations with the AER radiative transfer models, Journal of Geophysical Research: Atmospheres, 113, 1–8, https://doi.org/10.1029/2008JD009944, http://dx.doi.org/10.1029/2008JD009944, d13103, 2008.

Jenkin, M. E., Young, J. C., and Rickard, A. R.: The MCM v3.3.1 degradation scheme for isoprene, Atmospheric Chemistry and Physics, 15, 11 433–11 459, https://doi.org/10.5194/acp-15-11433-2015, 2015.

Jiao, C., Flanner, M. G., Balkanski, Y., Bauer, S. E., Bellouin, N., Berntsen, T. K., Bian, H., Carslaw, K. S., Chin, M., De Luca, N., Diehl, T., Ghan, S. J., Iversen, T., Kirkevag, A., Koch, D., Liu, X., Mann, G. W., Penner, J. E., Pitari, G., Schulz, M., Seland, O., Skeie, R. B., Steenrod, S. D., Stier, P., Takemura, T., Tsigaridis, K., van Noije, T., Yun, Y., and Zhang, K.: An AeroCom assessment of black carbon in Arctic snow and sea ice, Atmospheric Chemistry and Physics, 14, 2399–2417, https://doi.org/10.5194/acp-14-2399-2014, 2014.

Jöckel, P., Tost, H., Pozzer, A., Kunze, M., Kirner, O., Brenninkmeijer, C. A. M., Brinkop, S., Cai, D. S., Dyroff, C., Eckstein, J., Frank, F., Garny, H., Gottschaldt, K. D., Graf, P., Grewe, V., Kerkweg, A., Kern, B., Matthes, S., Mertens, M., Meul, S., Neumaier, M., Nutzel, M., Oberlander-Hayn, S., Ruhnke, R., Runde, T., Sander, R., Scharffe, D., and Zahn, A.: Earth System Chemistry integrated Modelling (ESCiMo) with the Modular Earth Submodel System (MESSy) version 2.51, Geoscientific Model Development, 9, 1153–1200, https://doi.org/10.5194/gmd-9-1153-2016, 2016.

Johnson, G. C., Lyman, J. M., and Loeb, N. G.: CORRESPONDENCE: Improving estimates of Earth's energy imbalance, Nature Climate Change, 6, 639–640, 2016.

JURECA, Jülich Supercomputing Centre.: JURECA: General-purpose supercomputer at Jülich Supercomputing Centre, Journal of large-scale research facilities, 2, 7, https://doi.org/10.17815/jlsrf-2-121, 2016.

Kaas, E., Guldberg, A., Déqué, M., Braun, A., Piedelievre, J., Guérémy, J., Machenhauer, B., Kirchner, I., D'Andrea, F., Vautard, R., et al.: Final report of the POTENTIALS project (Project On Tendency Evaluations using New Techniques to Improve Atmospheric Long-term Simulations), Available from the EU-Commision (DGXII), 2000.

Kinnison, D. E., Brasseur, G. P., Walters, S., Garcia, R. R., Marsh, D. R., Sassi, F., Harvey, V. L., Randall, C. E., Emmons, L., Lamarque, J. F., Hess, P., Orlando, J. J., Tie, X. X., Randel, W., Pan, L. L., Gettelman, A., Granier, C., Diehl, T., Niemeier, U., and Simmons, A. J.: Sensitivity of chemical tracers to meteorological parameters in the MOZART-3 chemical transport model, Journal of Geophysical Research-Atmospheres, 112, https://doi.org/10.1029/2006jd007879, 2007.

Kloster, S., Feichter, J., Reimer, E. M., Six, K. D., Stier, P., and Wetzel, P.: DMS cycle in the marine ocean-atmosphere system - a global model study, Biogeosciences, 3, 29–51, 2006.

Kokkola, H., Korhonen, H., Lehtinen, K. E. J., Makkonen, R., Asmi, A., Jarvenoja, S., Anttila, T., Partanen, A. I., Kulmala, M., Jarvinen, H., Laaksonen, A., and Kerminen, V. M.: SALSA - a sectional aerosol module for large scale applications, Atmospheric Chemistry and Physics, 8, 2469–2483, 2008.

Krefting, J.: Nudging in Climate Modeling with ECHAM6.3, Master thesis, Meteorological Institute, Rheinische Friedrich-Wilhelms-Universität Bonn, 2017.

Laepple, T., Schultz, M. G., Lamarque, J. F., Madronich, S., Shetter, R. E., Lefer, B. L., and Atlas, E.: Improved albedo formulation for chemistry transport models based on satellite observations and assimilated snow data and its impact on tropospheric photochemistry, Journal of Geophysical Research-Atmospheres, 110, https://doi.org/10.1029/2004jd005463, 2005.

Lamarque, J. F., Bond, T. C., Eyring, V., Granier, C., Heil, A., Klimont, Z., Lee, D., Liousse, C., Mieville, A., Owen, B., Schultz, M. G., Shindell, D., Smith, S. J., Stehfest, E., Van Aardenne, J., Cooper, O. R., Kainuma, M., Mahowald, N., McConnell, J. R., Naik, V., Riahi, K., and van Vuuren, D. P.: Historical (1850-2000) gridded anthropogenic and biomass burning emissions of reactive gases and aerosols: methodology and application, Atmospheric Chemistry and Physics, 10, 7017–7039, https://doi.org/10.5194/acp-10-7017-2010, 2010.

Lamarque, J. F., Emmons, L. K., Hess, P. G., Kinnison, D. E., Tilmes, S., Vitt, F., Heald, C. L., Holland, E. A., Lauritzen, P. H., Neu, J., Orlando, J. J., Rasch, P. J., and Tyndall, G. K.: CAM-chem: description and evaluation of interactive atmospheric chemistry in the Community Earth System Model, Geoscientific Model Development, 5, 369–411, https://doi.org/10.5194/gmd-5-369-2012, 2012.

Lana, A., Bell, T. G., Simo, R., Vallina, S. M., Ballabrera-Poy, J., Kettle, A. J., Dachs, J., Bopp, L., Saltzman, E. S., Stefels, J., Johnson, J. E., and Liss, P. S.: An updated climatology of surface dimethlysulfide concentrations and emission fluxes in the global ocean, Global Biogeochemical Cycles, 25, https://doi.org/10.1029/2010gb003850, 2011.

Levelt, P. F., Hilsenrath, E., Leppelmeier, G. W., van den Oord, G. H. J., Bhartia, P. K., Tamminen, J., de Haan, J. F., and Veefkind, J. P.: Science objectives of the ozone monitoring instrument, IEEE Transactions on Geoscience and Remote Sensing, 44, 1199–1208, https://doi.org/10.1109/TGRS.2006.872336, 2006.

Li, J. L. F., Waliser, D. E., Chen, W. T., Guan, B., Kubar, T., Stephens, G., Ma, H. Y., Deng, M., Donner, L., Seman, C., and Horowitz, L.: An observationally based evaluation of cloud ice water in CMIP3 and CMIP5 GCMs and contemporary reanalyses using contemporary satellite data, Journal of Geophysical Research-Atmospheres, 117, https://doi.org/10.1029/2012jd017640, 2012.

Liang, Q., Stolarski, R. S., Kawa, S. R., Nielsen, J. E., Douglass, A. R., Rodriguez, J. M., Blake, D. R., Atlas, E. L., and Ott, L. E.: Finding the missing stratospheric Br-y: a global modeling study of CHBr3 and CH2Br2, Atmospheric Chemistry and Physics, 10, 2269–2286, 2010.

Liao, H., Seinfeld, J. H., Adams, P. J., and Mickley, L. J.: Global radiative forcing of coupled tropospheric ozone and aerosols in a unified general circulation model, J. Geophys. Res., 109, https://doi.org/10.1029/2003JD004456, 2004.

Lin, S. J. and Rood, R. B.: Multidimensional flux-form semi-Lagrangian transport schemes, Monthly Weather Review, 124, 2046–2070, https://doi.org/10.1175/1520-0493(1996)124<2046:mffslt>2.0.co;2, 1996.

Livesey, N. J., Read, W. G., Wagner, P. A., Froidevaux, L., Lambert, A., Manney, G. L., Millán Valle, L. F., Pumphrey, H. C., Santee, M. L., Schwartz, M. J., Wang, S., Fuller, R. A., Jarnot, R. F., Knosp, B. W., and Martinez, E.: Version 4.2x Level 2 data quality and description document, Tech. rep., Jet Propulsion Laboratory, https://mls.jpl.nasa.gov/data/v4-2_data_quality_document.pdf, 2016.

Lohmann, U. and Hoose, C.: Sensitivity studies of different aerosol indirect effects in mixed-phase clouds, Atmospheric Chemistry and Physics, 9, 8917–8934, https://doi.org/10.5194/acp-9-8917-2009, https://www.atmos-chem-phys.net/9/8917/2009/, 2009.

Lohmann, U. and Roeckner, E.: Design and performance of a new cloud microphysics scheme developed for the ECHAM general circulation model, Climate Dynamics, 12, 557–572, https://doi.org/10.1007/s003820050128, 1996.

Lohmann, U., Stier, P., Hoose, C., Ferrachat, S., Kloster, S., Roeckner, E., and Zhang, J.: Cloud microphysics and aerosol indirect effects in the global climate model ECHAM5-HAM, Atmospheric Chemistry and Physics, 7, 3425–3446, https://doi.org/10.5194/acp-7-3425-2007, https://www.atmos-chem-phys.net/7/3425/2007/, 2007.

Long, M. S., Keene, W. C., Kieber, D. J., Erickson, D. J., and Maring, H.: A sea-state based source function for size- and composition-resolved marine aerosol production, Atmospheric Chemistry and Physics, 11, 1203–1216, https://doi.org/10.5194/acp-11-1203-2011, https://www.atmos-chem-phys.net/11/1203/2011/, 2011.

Lott, F.: Alleviation of stationary biases in a GCM through a mountain drag parameterization scheme and a simple representation of mountain lift forces, Monthly Weather Review, 127, 788–801, https://doi.org/10.1175/1520-0493(1999)127<0788:aosbia>2.0.co;2, 1999.

Meinshausen, M., Smith, S. J., Calvin, K., Daniel, J. S., Kainuma, M. L. T., Lamarque, J. F., Matsumoto, K., Montzka, S. A., Raper, S. C. B., Riahi, K., Thomson, A., Velders, G. J. M., and van Vuuren, D. P. P.: The RCP greenhouse gas concentrations and their extensions from 1765 to 2300, Climatic Change, 109, 213–241, https://doi.org/10.1007/s10584-011-0156-z, 2011.

Miller, B. R., Huang, J., Weiss, R. F., Prinn, R. G., and Fraser, P. J.: Atmospheric trend and lifetime of chlorodifluoromethane (HCFC-22) and the global tropospheric OH concentration, Journal of Geophysical Research-Atmospheres, 103, 13 237–13 248, https://doi.org/10.1029/98jd00771, 1998.

Miller, M. J., Palmer, T. N., and Swinbank, R.: Parametrization and influence of subgridscale orography in general circulation and numerical weather prediction models, Meteorol. Atmos. Phys., 40, 84–109, https://doi.org/10.1007/BF01027469, 1989.

Möbis, B. and Stevens, B.: Factors controlling the position of the Intertropical Convergence Zone on an aquaplanet, Journal of Advances in Modeling Earth Systems, 4, https://doi.org/10.1029/2012ms000199, 2012.

Morgenstern, O., Akiyoshi, H., Yamashita, Y., Kinnison, D. E., Garcia, R. R., Plummer, D. A., Scinocca, J., Zeng, G., Rozanov, E., Stenke, A., Revell, L. E., Pitari, G., Mancini, E., Di Genova, G., Dhomse, S. S., and Chipperfield, M. P.: Ozone sensitivity to varying greenhouse gases and ozone-depleting substances in CCMI simulations, Atmospheric Chemistry and Physics Discussions, in review, 1–32, https://doi.org/10.5194/acp-2017-565, 2017.

Naik, V., Voulgarakis, A., Fiore, A. M., Horowitz, L. W., Lamarque, J. F., Lin, M., Prather, M. J., Young, P. J., Bergmann, D., Cameron-Smith, P. J., Cionni, I., Collins, W. J., Dalsoren, S. B., Doherty, R., Eyring, V., Faluvegi, G., Folberth, G. A., Josse, B., Lee, Y. H., MacKenzie, I. A., Nagashima, T., van Noije, T. P. C., Plummer, D. A., Righi, M., Rumbold, S. T., Skeie, R., Shindell, D. T., Stevenson, D. S., Strode, S., Sudo, K., Szopa, S., and Zeng, G.: Preindustrial to present-day changes in tropospheric hydroxyl radical and methane lifetime from the Atmospheric Chemistry and Climate Model Intercomparison Project (ACCMIP), Atmospheric Chemistry and Physics, 13, 5277–5298, https://doi.org/10.5194/acp-13-5277-2013, 2013.

Neubauer, D., Lohmann, U., Hoose, C., and Frontoso, M. G.: Impact of the representation of marine stratocumulus clouds on the anthropogenic aerosol effect, Atmospheric Chemistry and Physics, 14, 11 997–12 022, https://doi.org/10.5194/acp-14-11997-2014, 2014.

Nordeng, T. E.: Extended versions of the convective parameterization scheme at ECMWF and their impact on the mean and transient activity of the model in the tropics, In Technical Memorandum, p. 41, Reading, UK, 1994.

Olson, J.: World ecosystems (WE1.4). Digital raster data on a 10 minute geographic 1080 × 2160 grid, in global ecosystems database ., disc A Version 1.0., 1992.

Palmer, T. N., Shutts, G. J., and Swinbank, R.: Alleviation of a systematic westerly bias in general circulation and numerical weather prediction models through an orographic gravity wave drag parametrization, Quarterly Journal of the Royal Meteorological Society, 112, 1001–1039, https://doi.org/10.1002/qj.49711247406, 1986.

Paulot, F., Crounse, J. D., Kjaergaard, H. G., Kurten, A., St Clair, J. M., Seinfeld, J. H., and Wennberg, P. O.: Unexpected Epoxide Formation in the Gas-Phase Photooxidation of Isoprene, Science, 325, 730–733, https://doi.org/10.1126/science.1172910, 2009.

PCMDI: AMIP Sea Surface Temperature and Sea Ice: Observational and Boundary Condition Data Sets, Web page, Lawrence Livermore National Laboratory, Livermoore, CA, http://www-pcmdi.llnl.gov/projects/amip/AMIP2EXPDSN/BCS/bcsintro.php, 2017.

Peeters, J., Nguyen, T. L., and Vereecken, L.: HOx radical regeneration in the oxidation of isoprene, Physical Chemistry Chemical Physics, 11, 5935–5939, https://doi.org/10.1039/b908511d, 2009.

Pickering, K. E., Wang, Y. S., Tao, W. K., Price, C., and Muller, J. F.: Vertical distributions of lightning NOx for use in regional and global chemical transport models, Journal of Geophysical Research-Atmospheres, 103, 31 203–31 216, https://doi.org/10.1029/98jd02651, 1998.

Pozzoli, L., Bey, I., Rast, S., Schultz, M. G., Stier, P., and Feichter, J.: Trace gas and aerosol interactions in the fully coupled model of aerosol-chemistry-climate ECHAM5-HAMMOZ: 1. Model description and insights from the spring 2001 TRACE-P experiment, Journal of Geophysical Research-Atmospheres, 113, https://doi.org/10.1029/2007jd009007, 2008a.

Pozzoli, L., Bey, I., Rast, S., Schultz, M. G., Stier, P., and Feichter, J.: Trace gas and aerosol interactions in the fully coupled model of aerosol-chemistry-climate ECHAM5-HAMMOZ: 2. Impact of heterogeneous chemistry on the global aerosol distributions, Journal of Geophysical Research-Atmospheres, 113, https://doi.org/10.1029/2007jd009008, 2008b.

Pozzoli, L., Janssens-Maenhout, G., Diehl, T., Bey, I., Schultz, M. G., Feichter, J., Vignati, E., and Dentener, F.: Re-analysis of tropospheric sulfate aerosol and ozone for the period 1980-2005 using the aerosol-chemistry-climate model ECHAM5-HAMMOZ, Atmospheric Chemistry and Physics, 11, 9563–9594, https://doi.org/10.5194/acp-11-9563-2011, 2011.

Prather, M. J., Holmes, C. D., and Hsu, J.: Reactive greenhouse gas scenarios: Systematic exploration of uncertainties and the role of atmospheric chemistry, Geophysical Research Letters, 39, https://doi.org/10.1029/2012gl051440, 2012.

Price, C. and Rind, D.: MODELING GLOBAL LIGHTNING DISTRIBUTIONS IN A GENERAL-CIRCULATION MODEL, Monthly Weather Review, 122, 1930–1939, https://doi.org/10.1175/1520-0493(1994)122<1930:mgldia>2.0.co;2, 1994.

Price, C., Penner, J., and Prather, M.: NOx from lightning .1. Global distribution based on lightning physics, Journal of Geophysical Research-Atmospheres, 102, 5929–5941, https://doi.org/10.1029/96jd03504, 1997.

Prinn, R. G., Huang, J., Weiss, R. F., Cunnold, D. M., Fraser, P. J., Simmonds, P. G., McCulloch, A., Harth, C., Reimann, S., Salameh, P., O'Doherty, S., Wang, R. H. J., Porter, L. W., Miller, B. R., and Krummel, P. B.: Evidence for variability of atmospheric hydroxyl radicals over the past quarter century, Geophysical Research Letters, 32, https://doi.org/10.1029/2004gl022228, 2005.

Rast, S., Schultz, M., Bey, I., van Noije, T., Aghedo, A., Brasseur, G., Diehl, T., Esch, M., Ganzeveld, L., Kirchner, I., Kornblueh, L., Rhodin, A., Roeckner, E., Schmidt, H., Schröder, S., Schulzweida, U., Stier, P., Thomas, K., and Walters, S.: Evaluation of the tropospheric chemistry general circulation model ECHAM5-MOZ and its application to the analysis of the chemical composition of the troposphere with an emphasis on the late RETRO period 1990-2000, Report, Max-Planck-Institut für Meteorologie, https://doi.org/doi:10.17617/2.2058065, 2014.

Reick, C. H., Raddatz, T., Brovkin, V., and Gayler, V.: Representation of natural and anthropogenic land cover change in MPI-ESM, Journal of Advances in Modeling Earth Systems, 5, 459–482, https://doi.org/10.1002/jame.20022, 2013.

Rodgers, C. D.: Inverse Methods for Atmospheric Sounding – Theory and Practice, World Scientific Publishing Co. Pte. Ltd, https://doi.org/10.1142/9789812813718, 2000.

Rodriguez, M. A. and Dabdub, D.: IMAGES-SCAPE2: A modeling study of size- and chemically resolved aerosol thermodynamics in a global chemical transport model, J. Geophys. Res., 109, https://doi.org/10.1029/2003JD003639, 2004.

Ronsmans, G., Langerock, B., Wespes, C., Hannigan, J. W., Hase, F., Kerzenmacher, T., Mahieu, E., Schneider, M., Smale, D., Hurtmans, D., De Mazière, M., Clerbaux, C., and Coheur, P.-F.: First characterization and validation of FORLI-HNO_3 vertical profiles retrieved from IASI/Metop, Atmospheric Measurement Techniques, 9, 4783–4801, https://doi.org/10.5194/amt-9-4783-2016, 2016.

Schultz, M. G., Akimoto, H., Bottenheim, J., Buchmann, B., Galbally, I. E., Gilge, S., Helmig, D., Koide, H., Lewis, A. C., Novelli, P. C., Plass-Dülmer, C., Ryerson, T. B., Steinbacher, M., Steinbrecher, R., Tarasova, O., Torseth, K., Thouret, V., and Zellweger, C.: The Global Atmosphere Watch reactive gases measurement network, Elementa: Science of the Anthropocene, 3, 1–23, https://doi.org/10.12952/journal.elementa.000067, 2015.

Schultz, M. G., Schröder, S., Lyapina, O., Cooper, O. R., Galbally, I., Petropavlovskikh, I., von Schneidemesser, E., Tanimoto, H., Elshorbany, Y., Naja, M., Seguel, R. J., Dauert, U., Eckhardt, P., Feigenspan, S., Fiebig, M., Hjellbrekke, A.-G., Hong, Y.-D., Kjeld, P. C., Koide, H., Lear, G., Tarasick, D., Ueno, M., Wallasch, M., Baumgardner, D., Chuang, M.-T., Gillett, R., Lee, M., Molloy, S., Moolla, R., Wang, T., Sharps, K., Adame, J. A., Ancellet, G., Apadula, F., Artaxo, P., Barlasina, M. E., Bogucka, M., Bonasoni, P., Chang, L., Colomb, A., Cuevas-Agulló, E., Cupeiro, M., Degorska, A., Ding, A., Fröhlich, M., Frolova, M., Gadhavi, H., Gheusi, F., Gilge, S., Gonzalez, M. Y., Gros, V., Hamad, S. H., Helmig, D., Henriques, D., Hermansen, O., Holla, R., Hueber, J., Im, U., Jaffe, D. A., Komala, N., Kubistin, D., Lam, K.-S., Laurila, T., Lee, H., Levy, I., Mazzoleni, C., Mazzoleni, L. R., McClure-Begley, A., Mohamad, M., Murovec, M., Navarro-Comas, M., Nicodim, F., Parrish, D., Read, K. A., Reid, N., Ries, L., Saxena, P., Schwab, J. J., Scorgie, Y., Senik, I., Simmonds, P., Sinha, V., Skorokhod, A. I., Spain, G., Spangl, W., Spoor, R., Springston, S. R., Steer, K., Steinbacher, M., Suharguniyawan, E., Torre, P., Trickl, T., Weili, L., Weller, R., Xu, X., Xue, L., and Zhiqiang, M.: Tropospheric Ozone Assessment Report: Database and Metrics Data of Global Surface Ozone Observations (in press.), Elementa, p. na., 2017.

Schumann, U. and Huntrieser, H.: The global lightning-induced nitrogen oxides source, Atmospheric Chemistry and Physics, 7, 3823–3907, 2007.

Solomon, S.: Stratospheric ozone depletion: A review of concepts and history, Reviews of Geophysics, 37, 275–316, https://doi.org/10.1029/1999RG900008, 1999.

Solomon, S., Kinnison, D., Bandoro, J., and Garcia, R.: Simulation of polar ozone depletion: An update, Journal of Geophysical Research: Atmospheres, 120, 7958–7974, https://doi.org/10.1002/2015JD023365, 2015JD023365, 2015.

SPARC: SPARC CCMVal Report on the Evaluation of Chemistry-Climate Models, Tech. rep., SPARC, http://www.sparc-climate.org/publications/sparc-reports/, 2010.

Stadtler, S., Simpson, D., Schröder, S., Taraborrelli, D., Bott, A., and Schultz, M.: Ozone Impacts of Gas-Aerosol Uptake in Global Chemistry Transport Models, Atmos. Chem. Phys. Discuss., 2017, 1–35, https://doi.org/10.5194/acp-2017-566, https://www.atmos-chem-phys-discuss.net/acp-2017-566/, 2017.

Stanelle, T., Bey, I., Raddatz, T., Reick, C., and Tegen, I.: Anthropogenically induced changes in twentieth century mineral dust burden and the associated impact on radiative forcing, Journal of Geophysical Research-Atmospheres, 119, 13 526–13 546, https://doi.org/10.1002/2014jd022062, 2014.

Stein, O., Schultz, M. G., Bouarar, I., Clark, H., Huijnen, V., Gaudel, A., George, M., and Clerbaux, C.: On the wintertime low bias of Northern Hemisphere carbon monoxide found in global model simulations, Atmos. Chem. Phys., 14, 9295–9316, https://doi.org/10.5194/acp-14-9295-2014, 2014.

Stevens, B., Giorgetta, M., Esch, M., Mauritsen, T., Crueger, T., Rast, S., Salzmann, M., Schmidt, H., Bader, J., Block, K., Brokopf, R., Fast, I., Kinne, S., Kornblueh, L., Lohmann, U., Pincus, R., Reichler, T., and Roeckner, E.: Atmospheric component of the MPI-M Earth System Model: ECHAM6, Journal of Advances in Modeling Earth Systems, 5, 146–172, https://doi.org/10.1002/jame.20015, 2013.

Stevenson, D. S., Dentener, F. J., Schultz, M. G., Ellingsen, K., van Noije, T. P. C., Wild, O., Zeng, G., Amann, M., Atherton, C. S., Bell, N., Bergmann, D. J., Bey, I., Butler, T., Cofala, J., Collins, W. J., Derwent, R. G., Doherty, R. M., Drevet, J., Eskes, H. J., Fiore, A. M., Gauss, M., Hauglustaine, D. A., Horowitz, L. W., Isaksen, I. S. A., Krol, M. C., Lamarque, J. F., Lawrence, M. G., Montanaro, V., Muller, J. F., Pitari, G., Prather, M. J., Pyle, J. A., Rast, S., Rodriguez, J. M., Sanderson, M. G., Savage, N. H., Shindell, D. T., Strahan, S. E., Sudo, K., and Szopa, S.: Multimodel ensemble simulations of present-day and near-future tropospheric ozone, Journal of Geophysical Research-Atmospheres, 111, https://doi.org/10.1029/2005jd006338, 2006.

Stier, P., Feichter, J., Kinne, S., Kloster, S., Vignati, E., Wilson, J., Ganzeveld, L., Tegen, I., Werner, M., Balkanski, Y., Schulz, M., Boucher, O., Minikin, A., and Petzold, A.: The aerosol-climate model ECHAM5-HAM, Atmospheric Chemistry and Physics, 5, 1125–1156, 2005.

Stubenrauch, C. J., Rossow, W. B., Kinne, S., Ackerman, S., Cesana, G., Chepfer, H., Di Girolamo, L., Getzewich, B., Guignard, A., Heidinger, A., Maddux, B. C., Menzel, W. P., Minnis, P., Pearl, C., Platnick, S., Poulsen, C., Riedi, J., Sun-Mack, S., Walther, A., Winker, D., Zeng, S., and Zhao, G.: Assessment of Global Cloud Datasets from Satellites: Project and Database Initiated by the GEWEX Radiation Panel, Bulletin of the American Meteorological Society, 94, 1031–1049, https://doi.org/10.1175/bams-d-12-00117.1, 2013.

Sundqvist, H., Berge, E., and Kristjansson, J. E.: CONDENSATION AND CLOUD PARAMETERIZATION STUDIES WITH A MESOSCALE NUMERICAL WEATHER PREDICTION MODEL, Monthly Weather Review, 117, 1641–1657, https://doi.org/10.1175/1520-0493(1989)117<1641:cacpsw>2.0.co;2, 1989.

Té, Y., Jeseck, P., Franco, B., Mahieu, E., Jones, N., Paton-Walsh, C., Griffith, D. W. T., Buchholz, R. R., Hadji-Lazaro, J., Hurtmans, D., and Janssen, C.: Seasonal variability of surface and column carbon monoxide over the megacity Paris, high-altitude Jungfraujoch and Southern Hemispheric Wollongong stations, Atmos. Chem. Phys., 16, 10 911–10 925, https://doi.org/10.5194/acp-16-10911-2016, 2016.

Taraborrelli, D., Lawrence, M. G., Butler, T. M., Sander, R., and Lelieveld, J.: Mainz Isoprene Mechanism 2 (MIM2): an isoprene oxidation mechanism for regional and global atmospheric modelling, Atmospheric Chemistry and Physics, 9, 2751–2777, 2009.

Textor, C., Schulz, M., Guibert, S., Kinne, S., Balkanski, Y., Bauer, S., Berntsen, T., Berglen, T., Boucher, O., Chin, M., Dentener, F., Diehl, T., Easter, R., Feichter, H., Fillmore, D., Ghan, S., Ginoux, P., Gong, S., Kristjansson, J. E., Krol, M., Lauer, A., Lamarque, J. F., Liu, X., Montanaro, V., Myhre, G., Penner, J., Pitari, G., Reddy, S., Seland, O., Stier, P., Takemura, T., and Tie, X.: Analysis and quantification of the diversities of aerosol life cycles within AeroCom, Atmos. Chem. Phys., 6, 1777–1813, 2006.

Tiedtke, M.: A COMPREHENSIVE MASS FLUX SCHEME FOR CUMULUS PARAMETERIZATION IN LARGE-SCALE MODELS, Monthly Weather Review, 117, 1779–1800, https://doi.org/10.1175/1520-0493(1989)117<1779:acmfsf>2.0.co;2, 1989.

Tilmes, S., Lamarque, J. F., Emmons, L. K., Conley, A., Schultz, M. G., Saunois, M., Thouret, V., Thompson, A. M., Oltmans, S. J., Johnson, B., and Tarasick, D.: Technical Note: Ozonesonde climatology between 1995 and 2011: description, evaluation and applications, Atmospheric Chemistry and Physics, 12, 7475–7497, https://doi.org/10.5194/acp-12-7475-2012, 2012.

Tilmes, S., Lamarque, J. F., Emmons, L. K., Kinnison, D. E., Marsh, D., Garcia, R. R., Smith, A. K., Neely, R. R., Conley, A., Vitt, F., Martin, M. V., Tanimoto, H., Simpson, I., Blake, D. R., and Blake, N.: Representation of the Community Earth System Model (CESM1) CAM4-chem within the Chemistry-Climate Model Initiative (CCMI), Geoscientific Model Development, 9, 1853–1890, https://doi.org/10.5194/gmd-9-1853-2016, 2016.

van Vuuren, D. P., Edmonds, J., Kainuma, M., Riahi, K., Thomson, A., Hibbard, K., Hurtt, G. C., Kram, T., Krey, V., Lamarque, J. F., Masui, T., Meinshausen, M., Nakicenovic, N., Smith, S. J., and Rose, S. K.: The representative concentration pathways: an overview, Climatic Change, 109, 5–31, https://doi.org/10.1007/s10584-011-0148-z, 2011.

Vignati, E., Wilson, J., and Stier, P.: M7: An efficient size-resolved aerosol microphysics module for large-scale aerosol transport models, Journal of Geophysical Research-Atmospheres, 109, https://doi.org/10.1029/2003jd004485, 2004.

von der Haar, T. H., Bytheway, J. L., and Forsythe, J. M.: Weather and climate analyses using improved global water vapor observations, Geophysical Research Letters, 39, https://doi.org/10.1029/2012gl052094, 2012.

Wesely, M. L.: PARAMETERIZATION OF SURFACE RESISTANCES TO GASEOUS DRY DEPOSITION IN REGIONAL-SCALE NUMERICAL-MODELS, Atmospheric Environment, 23, 1293–1304, https://doi.org/10.1016/0004-6981(89)90153-4, 1989.

Wespes, C., Hurtmans, D., Emmons, L. K., Safieddine, S., Clerbaux, C., Edwards, D. P., and Coheur, P.-F.: Ozone variability in the troposphere and the stratosphere from the first 6 years of IASI observations (2008–2013), Atmospheric Chemistry and Physics, 16, 5721–5743, https://doi.org/10.5194/acp-16-5721-2016, 2016.

Wespes, C., Hurtmans, D., Clerbaux, C., and Coheur, P.-F.: O3 variability in the troposphere as observed by IASI over 2008–2016: Contribution of atmospheric chemistry and dynamics, Journal of Geophysical Research: Atmospheres, 122, 2429–2451, https://doi.org/10.1002/2016JD025875, http://dx.doi.org/10.1002/2016JD025875, 2016JD025875, 2017.

Wild, M., Folini, D., Schar, C., Loeb, N., Dutton, E. G., and Konig-Langlo, G.: The global energy balance from a surface perspective, Climate Dynamics, 40, 3107–3134, https://doi.org/10.1007/s00382-012-1569-8, 2013.

WMO, (World Meteorological Organization).: Scientific Assessment of Ozone Depletion: 2010, Global Ozone Research and Monitoring Project-Report No. 52, p. 516, https://www.esrl.noaa.gov/csd/assessments/ozone/2010/, Geneva, Switzerland, 2011.

WMO, (World Meteorological Organization).: Scientific Assessment of Ozone Depletion: 2014, Global Ozone Research and Monitoring Project-Report No. 55, p. 416, https://www.esrl.noaa.gov/csd/assessments/ozone/2014/, Geneva, Switzerland, 2014.

Wofsy, S. C., Team, H. S., Cooperating Modellers, T., and Satellite, T.: HIAPER Pole-to-Pole Observations (HIPPO): fine-grained, global-scale measurements of climatically important atmospheric gases and aerosols, Philosophical Transactions of the Royal Society a-Mathematical Physical and Engineering Sciences, 369, 2073–2086, https://doi.org/10.1098/rsta.2010.0313, 2011.

Wolfe, G. M., Crounse, J. D., Parrish, J. D., St Clair, J. M., Beaver, M. R., Paulot, F., Yoon, T. P., Wennberg, P. O., and Keutsch, F. N.: Photolysis, OH reactivity and ozone reactivity of a proxy for isoprene-derived hydroperoxyenals (HPALDs), Physical Chemistry Chemical Physics, 14, 7276–7286, https://doi.org/10.1039/c2cp40388a, 2012.

Xu, L. and Penner, J. E.: Global simulations of nitrate and ammonium aerosols and their radiative effects, Atmospheric Chemistry and Physics, 12, 9479–9504, https://doi.org/10.5194/acp-12-9479-2012, 2012.

Young, A. H., Keene, W. C., Pszenny, A. A. P., Sander, R., Thornton, J. A., Riedel, T. P., and Maben, J. R.: Phase partitioning of soluble trace gases with size-resolved aerosols in near-surface continental air over northern Colorado, USA, during winter, Journal of Geophysical Research-Atmospheres, 118, 9414–9427, https://doi.org/10.1002/jgrd.50655, 2013.

Zhang, K., O'Donnell, D., Kazil, J., Stier, P., Kinne, S., Lohmann, U., Ferrachat, S., Croft, B., Quaas, J., Wan, H., Rast, S., and Feichter, J.: The global aerosol-climate model ECHAM-HAM, version 2: sensitivity to improvements in process representations, Atmospheric Chemistry and Physics, 12, 8911–8949, https://doi.org/10.5194/acp-12-8911-2012, 2012.

Zhang, K., Wan, H., Liu, X., Ghan, S. J., Kooperman, G. J., Ma, P. L., Rasch, P. J., Neubauer, D., and Lohmann, U.: Technical Note: On the use of nudging for aerosol-climate model intercomparison studies, Atmos. Chem. Phys., 14, 8631–8645, https://doi.org/10.5194/acp-14-8631-2014, https://www.atmos-chem-phys.net/14/8631/2014/, 2014.

Zhang, S. P., Wang, M. H., Ghan, S. J., Ding, A. J., Wang, H. L., Zhang, K., Neubauer, D., Lohmann, U., Ferrachat, S., Takeamura, T., Gettelman, A., Morrison, H., Lee, Y., Shindell, D. T., Partridge, D. G., Stier, P., Kipling, Z., and Fu, C. B.: On the characteristics of aerosol indirect effect based on dynamic regimes in global climate models, Atmospheric Chemistry and Physics, 16, 2765–2783, https://doi.org/10.5194/acp-16-2765-2016, 2016.